iScience

Article

APOE4 drives widespread changes to the hepatic proteome and alters metabolic function

Graphical abstract

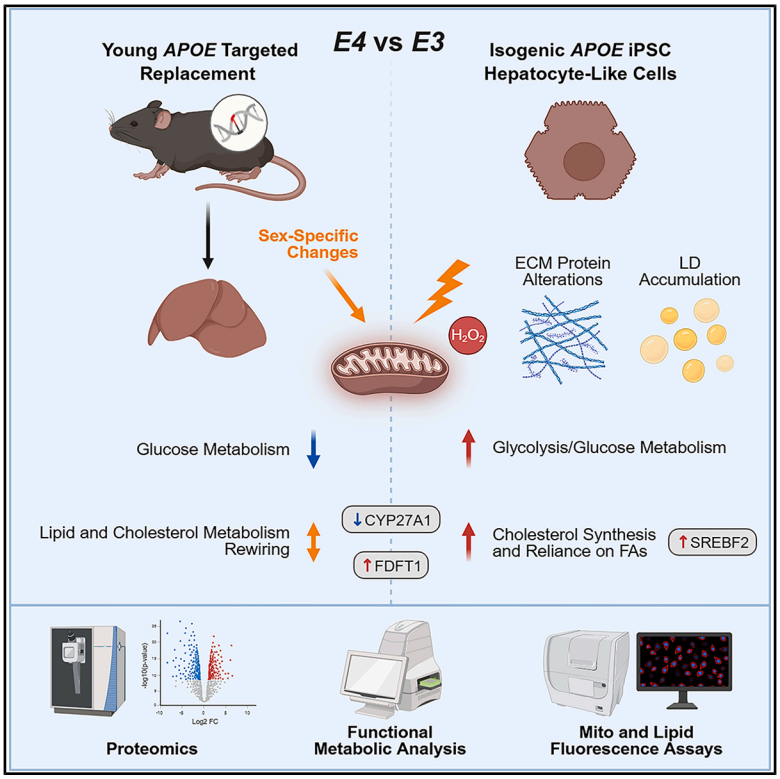

Highlights

- *APOE4* alters the liver proteome and mitochondrial function in young mice
- Glycolysis and glucose metabolism are upregulated in *APOE4* iHLCs
- *APOE4* increases fatty acid reliance in iHLCs and causes lipid droplet accumulation
- Cholesterol metabolism proteins are altered by *APOE4* in mouse livers and iHLCs

Authors

Colton R. Lysaker, Chelsea N. Johnson, Vivien Csikos, ..., Paige C. Geiger, Jill K. Morris, Heather M. Wilkins

Correspondence

hwilkins@kumc.edu

In brief

Biochemistry; Human metabolism; Proteomics

Lysaker et al., 2026, iScience *29*, 115035
March 20, 2026
https://doi.org/10.1016/j.isci.2026.115035

CellPress

iScience

CellPress
OPEN ACCESS

Article

APOE4 drives widespread changes to the hepatic proteome and alters metabolic function

Colton R. Lysaker,[1,2] Chelsea N. Johnson,[2,3] Vivien Csikos,[1,2] Edziu Franczak,[3,4,5] Ashley L. Tetlow,[1,2] Maggie Benson,[1,2] John P. Thyfault,[2,3,4,5,6] Paige C. Geiger,[3,5] Jill K. Morris,[1,2] and Heather M. Wilkins[1,2,7,8,*]

[1]Department of Neurology, University of Kansas Medical Center, Kansas City, KS, USA
[2]University of Kansas Alzheimer's Disease Research Center, Kansas City, KS, USA
[3]Department of Cell Biology and Physiology, University of Kansas Medical Center, Kansas City, KS, USA
[4]Kansas Center for Metabolism and Obesity Research, University of Kansas Medical Center, Kansas City, KS, USA
[5]Diabetes Institute, University of Kansas Medical Center, Kansas City, KS, USA
[6]Department of Internal Medicine, University of Kansas Medical Center, Kansas City, KS, USA
[7]Department of Biochemistry and Molecular Biology, University of Kansas Medical Center, Kansas City, KS, USA
[8]Lead contact
*Correspondence: hwilkins@kumc.edu
https://doi.org/10.1016/j.isci.2026.115035

SUMMARY

Apolipoprotein E (APOE) is essential for lipid homeostasis and has been extensively studied in Alzheimer's disease (AD). Individuals carrying an *APOE4* allele have an increased risk of AD and exhibit deficits in energy metabolism, including glucose utilization and mitochondrial dysfunction. While the role of APOE in the liver is well characterized, the impact of *APOE* genotype on hepatic health and metabolism remains poorly understood. We sought to investigate this using young *APOE3* and *APOE4*-targeted replacement mice and isogenic-induced pluripotent stem cell (iPSC)-derived hepatocyte-like cells (iHLCs). Proteomic and functional assays show that *APOE4* causes extensive changes to liver mitochondrial function in a sex-specific manner in mice and alters glucose and lipid metabolism. *APOE4* also impairs mitochondrial function in iHLCs, shifts metabolism towards glycolysis, increases reliance on fatty acid utilization, and drives lipid accumulation. Together, these findings show that *APOE* genetic variation causes mitochondrial dysfunction and rewires hepatic metabolism.

INTRODUCTION

Apolipoprotein E (APOE) is essential for lipid transport and metabolism. Genetic variation in *APOE* not only influences lipid homeostasis but also modulates the risk of developing late onset Alzheimer's disease (LOAD).[1] *APOE* is polymorphic, and variation in *APOE* genotype includes alleles that either confer decreased (*APOE**ε2*), neutral (*APOE**ε3*), or increased (*APOE**ε4*) risk of Alzheimer's disease (AD).[1,2] These alleles give rise to the APOE2, APOE3, and APOE4 protein isoforms, which differ in their receptor and lipid-binding preferences.[3,4] APOE2 and APOE3 primarily associate with high-density lipoproteins (HDLs), commonly referred to as "good cholesterol," while APOE4 preferentially binds to very low-density lipoproteins (VLDLs), known as a "bad cholesterol."[3] Within the human population, *APOE3* is the most common allele with *APOE2* and *APOE4* being less common.[5] While considerable focus has been placed on how *APOE* genetic variation affects brain health, much remains unknown regarding its impact on the liver.

Across the body there are two distinct pools of APOE production. This includes the central nervous system (CNS) and the liver, which are separated by the blood-brain barrier (BBB).[6,7] In the periphery, APOE is primarily produced and secreted by hepatocytes.[8,9] Once secreted, APOE binds nascent lipoprotein particles and transports lipids to distal tissues for use.[10,11] The importance of APOE in the liver and other tissues has been highlighted by studies in mice where knockout (KO) of *Apoe* results in significant metabolic stress, specifically dyslipidemia, atherosclerosis, oxidative stress, and inflammation.[12–14] One particular study examined mitochondrial proteomic changes in *Apoe* deficient mice and found upregulation of proteins associated with lipid metabolism and downregulation of proteins associated with the antioxidant response.[15] This not only highlights the importance of APOE in broad metabolic function but also its potential effects on mitochondria.

Only a few studies have examined the role of APOE isoforms on hepatic metabolism including work in both *in vivo* and *in vitro* models. Of these limited studies, one investigated how APOE isoforms influence hepatic metabolism in female *APOE*-targeted replacement (TR) mice and transformed Huh-7 hepatoma cells expressing APOE3 or APOE4.[16] Their results showed that APOE4 altered liver proteasome activity and decreased

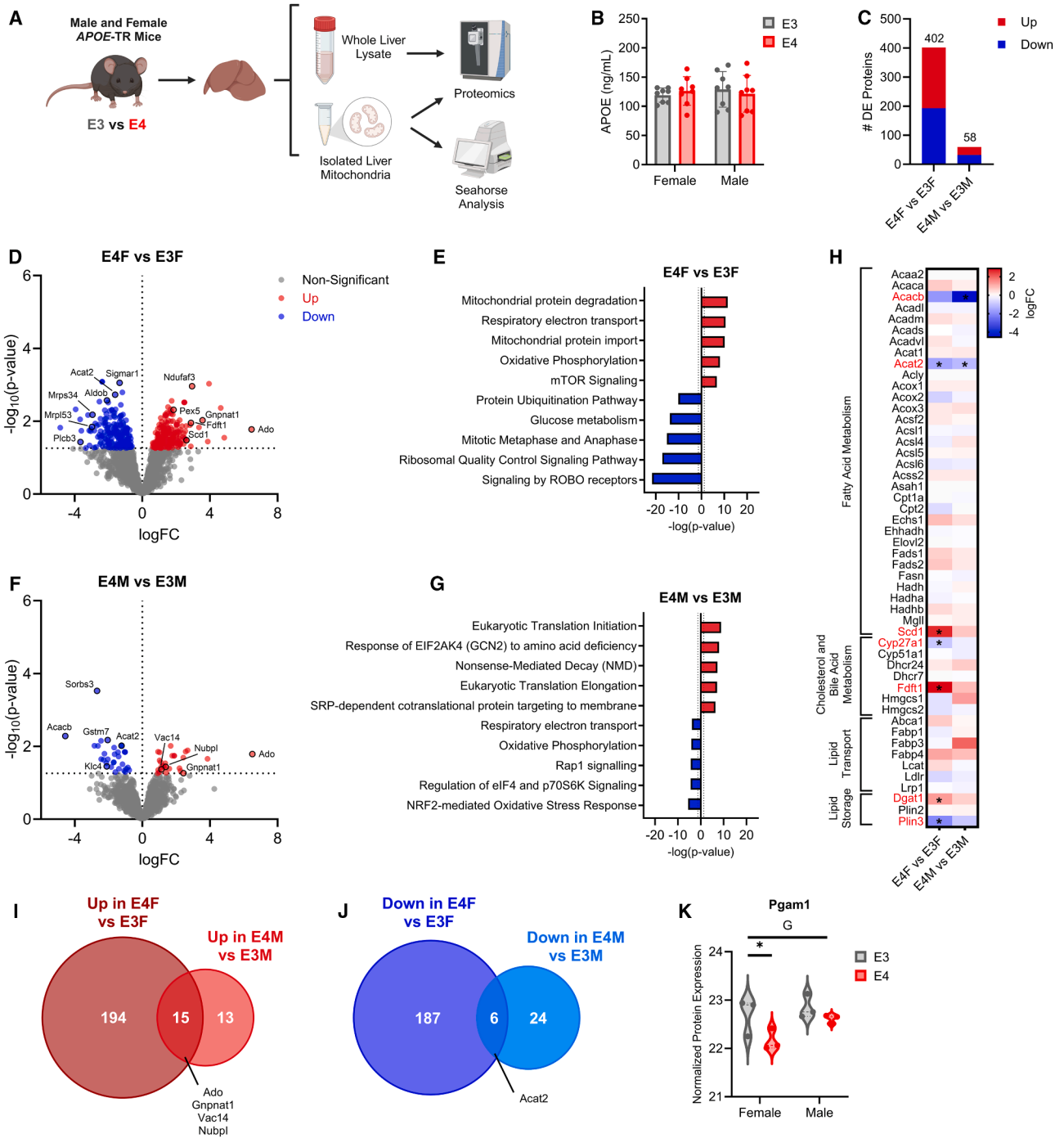

Figure 1. Whole liver proteomics in female and male APOE3 and APOE4 mice

(A) Study schematic showing primary outcomes in *APOE*-targeted replacement (TR) mice. *n* = 3 mice per group for all mouse proteomic outcomes.

(B) APOE protein expression from whole liver measured via ELISA in male and female *APOE3* and *APOE4* mice. Statistical significance was determined by two-way ANOVA. Data are presented as mean ± SD. *n* = 8 mice per genotype and sex.

(C) The number of differentially expressed (DE) proteins in male and female *APOE3* and *APOE4* mice.

(D) Volcano plot showing upregulated and downregulated proteins in female *APOE4* vs. *APOE3* mice.

(E) IPA pathway showing top 5 upregulated and downregulated pathways in female *APOE4* vs. *APOE3* mice.

(F) Volcano plot showing upregulated and downregulated proteins in male *APOE4* vs. *APOE3* mice.

(G) IPA pathway analysis showing top 5 upregulated and downregulated pathways in male *APOE4* vs. *APOE3* mice.

(legend continued on next page)

adenosine triphosphate (ATP) levels under stress in Huh-7 cells. Despite this, they observed little change to proteins associated with mitochondrial function and autophagy. However, proteomic work in male *APOE*-TR mice on a western diet found that APOE4 protects against diet-induced changes to the liver when compared to APOE3.[17] They also showed that *APOE* genotype-altered proteins associated with immune response, ER stress, and metabolic function in the liver. Another group found that differences in *APOE* genotype can alter lipidomic profiles in primary human hepatocytes.[18] More recently, a serum proteomic analysis in individuals with AD highlighted peripheral protein changes influenced by *APOE* genotype, with several of these proteins secreted by the liver.[19]

In this study we investigated how *APOE* genetic variation, specifically *E3* versus *E4* genotypes, impacts hepatic metabolism via unbiased proteomic analysis and mitochondrial respirometry in 4-month-old *APOE*-TR mice and induced pluripotent stem cell (iPSC)-derived hepatocyte-like cells (iHLCs). To our knowledge, this is the first study to leverage iHLCs to investigate the role of *APOE* genotype in hepatic metabolism *in vitro*. Based on past research, we hypothesized that APOE would drive changes to hepatic metabolism, where *APOE4* models would show mitochondrial dysfunction and upregulated glycolytic flux. Our findings show that *APOE* genetic variation alters the hepatic proteome and modifies metabolic function in both *APOE*-TR mice and isogenic iHLCs.

RESULTS

APOE genotype and sex alter the hepatic proteome in young mice

Four-month-old male and female *APOE*3 or *APOE*4-TR mice (n = 8 per genotype/sex) were used to examine whole liver and isolated mitochondrial proteomics in addition to Seahorse mitochondrial function assays (Figure 1A). We first examined whole liver protein expression of APOE between male and female *APOE3* and *APOE4* mice and observed no difference at 4 months (Figure 1B). Whole liver proteomics revealed 402 differently expressed (DE) proteins between female *APOE4* and *APOE3* mice versus only 58 DE proteins between male *APOE4* and *APOE3* mice (Figure 1C). In both comparisons ~50% of the proteins were DE up in E4 or down in E4. Female *APOE4*-TR mice when compared to female *APOE3*-TR mice had increased expression of proteins involved in cellular bioenergetics (Ndufaf3, Fdft1, Scd1, Ado, and Gnpnat1) and peroxisomal function (Pex5) with reduced expression of proteins involved in cholesterol metabolism (Acat2), glycolysis/gluconeogenesis (Aldob), mitochondrial ribosomal function (Mrps34 and Mrpl53), mitochondrial/ER interactions/autophagy (Sigmar1), and cell signaling (Plcb3) (Figure 1D). Ingenuity pathway analysis (IPA) revealed significant upregulation of mitochondrial protein degradation, electron transport in the respiratory chain/oxidative phosphorylation, mitochondrial protein import, and mechanistic target of rapamycin (mTOR) signaling pathways in *APOE4* female TR mice when compared to their *APOE3* counterparts (Figure 1E). Downregulated pathways in *APOE4* vs. *E3* female mice included protein ubiquitination, glucose metabolism, mitotic metaphase and anaphase, ribosomal quality control, and roundabout (ROBO) signaling pathways (Figure 1E).

Male *APOE4* mice had increased expression of proteins involved in cellular bioenergetics (Ado, Nubpl, and Gnpnat1) and lysosomal function (Vac14) with reduced expression of proteins involved in cholesterol metabolism (Acat2 and Acacb), antioxidant defense (Gstm7), and autophagy or microtubule/actin signaling (Sorbs3 and Klf4) when compared to *APOE3* mice (Figure 1F). IPA revealed a significant upregulation of eukaryotic translation initiation, amino acid deficiency, nonsense-mediated decay, eukaryotic translation elongation, and signal recognition particle (SRP)-dependent co-translational protein targeting pathways in male *APOE4* mice (Figure 1G). Downregulated pathways included oxidative phosphorylation, Rap1 signaling, regulation of eIF4/p70S6K, and NRF2 oxidative stress response pathways in *APOE4* male mice (Figure 1G).

Sex-specific differences were observed irrespective of *APOE* genotype in the mice (Figure S1). Notably, *APOE3* male mice exhibited an increase in peroxisomal lipid metabolism compared to their female counterparts (Figure S1D). To examine sex-specific differences in lipid proteins, we generated a heatmap of fatty acid metabolism, cholesterol metabolism, and lipid-related pathways. Further analysis of fatty acid proteins in mice revealed decreased expression of Acat2 in both male and female *APOE4* mice compared to their *APOE3* counterparts, with Acacb exhibiting decreased expression in male *APOE4* mice only (Figure 1H). Furthermore, female *APOE4* mice had upregulation of Scd1 (Figure 1H). Cholesterol and bile acid metabolism revealed decreased Cyp27a1 expression in *APOE4* female mice with an upregulation Fdft1 (Figure 1H). Lipid storage pathway protein Dgat1 was upregulated while Plin3 was downregulated in female *APOE4* mice (Figure 1H). Female and male mice shared 15 upregulated proteins and 6 downregulated proteins when compared between *APOE4* and *APOE3* mice (Figures 1I and 1J). These findings highlight the sex-specific effects of *APOE* genotype on liver proteomics. Given the changes in glucose metabolism and related pathways, we assessed glycolytic enzyme levels and observed a downregulation of Pgam1, which catalyzes the conversion of 3-phosphoglycerate to 2-phosphoglycerate and contributes to glycolytic flux, in *APOE4* mice (Figure 1K).

(H) Heatmap of proteins involved in fatty acid metabolism, cholesterol and bile acid metabolism, lipid transport, and lipid storage showing upregulated and downregulated proteins between *APOE4* and *APOE3* mice.

(I) Venn diagram showing the number of shared upregulated proteins between comparisons of female *APOE4* vs. *APOE3* mice and male *APOE4* vs. *APOE3* mice.

(J) Venn diagram showing the number of downregulated proteins shared between comparisons of female *APOE4* vs. *APOE3* mice and male *APOE4* vs. *APOE3* mice.

(K) Violin plot showing normalized Pgam1 protein expression from liver proteomics in male and female *APOE3* and *APOE4* mice. Statistical significance was determined by two-way ANOVA with Fisher's LSD post hoc. $^*p < 0.05$. G, genotype. n = 3 mice per genotype and sex.

See also Figure S1.

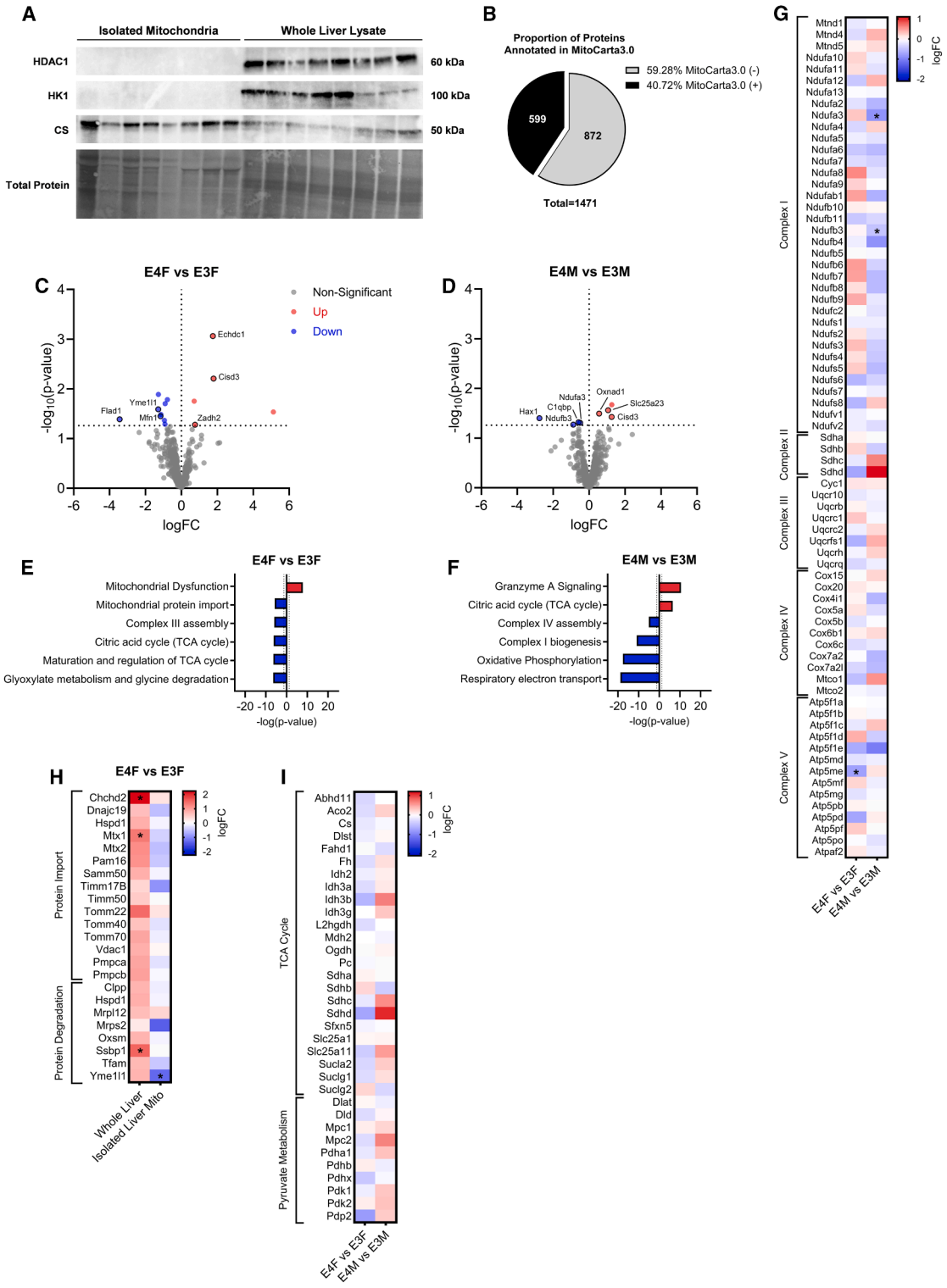

Figure 2. Isolated liver mitochondrial proteomics in male and female *APOE3* or *APOE4* mice

(A) Western blot analysis assessing purity of liver mitochondrial isolates. Blots were probed for HDAC1, HK1, and CS.

(B) Pie chart showing the proportion of proteins identified in isolated liver mitochondrial samples that are annotated as mitochondrial in the MitoCarta3.0 database.

(C) Volcano plot showing upregulated and downregulated proteins between female *APOE4* and *APOE3* mice.

(legend continued on next page)

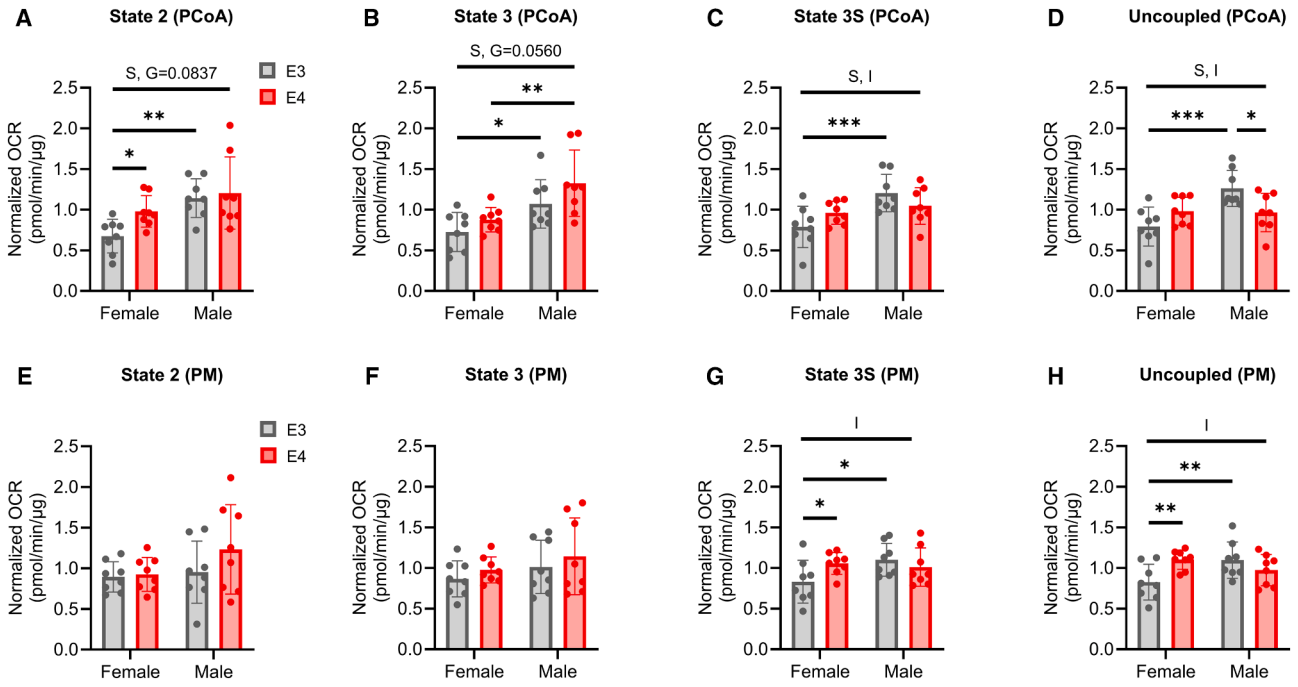

Figure 3. Mitochondrial respiration from isolated liver mitochondria in male and female APOE3 and APOE4 mice

(A–D) Fatty acid-driven respiration (palmitoyl-carnitine; PCoA) measured at state 2 (A), state 3 (B), state 3S (C), and uncoupled respiration (D).

(E–H) Carbohydrate-driven respiration (pyruvate and malate; PM) measured at state 2 (E), state 3 (F), state 3S (G), and uncoupled respiration (H). (A–H) Statistical significance was determined by two-way ANOVA with Fisher's LSD post hoc. Data shown as mean ± SD. *$p < 0.05$, **$p < 0.01$, ***$p < 0.001$. S = sex, G = genotype, I = interaction. $n = 8$ mice per genotype and sex.

Mitochondrial proteins and pathways are modified by APOE genotype and sex

We next examined isolated mitochondrial proteomics from *APOE*-TR mice liver samples. To validate our mitochondrial isolation, we first performed western blot analysis on isolated liver mitochondria and compared them to whole liver lysates (Figure 2A). The nuclear marker histone deacetylase 1 (HDAC1) and cytosolic marker hexokinase 1 (HK1) were detected only in whole liver lysates, while the mitochondrial marker citrate synthase (CS) was present in both preparations, confirming successful mitochondrial enrichment (Figure 2A). Before any proteomic analysis was performed, we cross-referenced the isolated mitochondria protein library with MitoCarta3.0.[20] Of the 1,471 proteins identified in the isolated mitochondria, 599 (40.72%) were annotated in MitoCarta3.0 (Figure 2B). Notably, while cytosolic markers were absent by western blot, close to only half of the identified proteins were annotated in MitoCarta3.0, likely due to the high sensitivity of mass spectrometry detecting low-abundance contaminants and proteins loosely associated with mitochondria.

Female *APOE4* mice had increased expression of fatty acid beta-oxidation (FAO) proteins (Zadh2 and Echdc1), and proteins involved in regulating reactive oxygen species (ROS), electron transport, and oxidative phosphorylation (Cisd3) (Figure 2C). The mitochondrial dynamic protein involved in fusion Mfn1, FAD production protein Flad1, and mitochondrial protease Yme1l1 were downregulated in *APOE4* female mice (Figure 2C). Male *APOE4* mice had increased expression of DNA repair proteins (Oxnad1), mitochondrial calcium homeostasis proteins (Slc25a23), and proteins involved in regulating ROS, electron transport, and oxidative phosphorylation (Cisd3) (Figure 2D). Mitochondrial complex I proteins Ndufa3 and Ndufb3, apoptotic regulator Hax1, and complement protein C1qbp were downregulated in male *APOE4* mice (Figure 2D). Female *APOE4* mice showed an upregulation in the mitochondrial dysfunction pathway but a downregulation in mitochondrial protein import, complex III assembly, TCA cycle, and glyoxylate metabolism, and glycine degradation pathways (Figure 2E). Male *APOE4* mice showed an upregulation in granzyme A signaling and TCA cycle pathways, but a downregulation in complex IV assembly, complex I biogenesis, oxidative

(D) Volcano plot showing upregulated and downregulated proteins between male *APOE4* and *APOE3* mice.

(E) IPA pathway analysis showing top upregulated and downregulated pathways between female *APOE4* and *APOE3* mice.

(F) IPA pathway analysis showing top upregulated and downregulated pathways between male *APOE4* and *APOE3* mice.

(G) Heatmap of oxidative phosphorylation complex I–V components between *APOE4* and *APOE3* female and male mice. $n = 3$ for proteomic outcomes.

(H) Heatmap comparing whole liver to isolated mitochondria results of proteins involved in mitochondrial protein import and degradation between *APOE4* and *APOE3* female mice.

(I) Heatmap of proteins involved in TCA cycle and pyruvate metabolism between *APOE4* and *APOE3* female and male mice.

See also Figure S2.

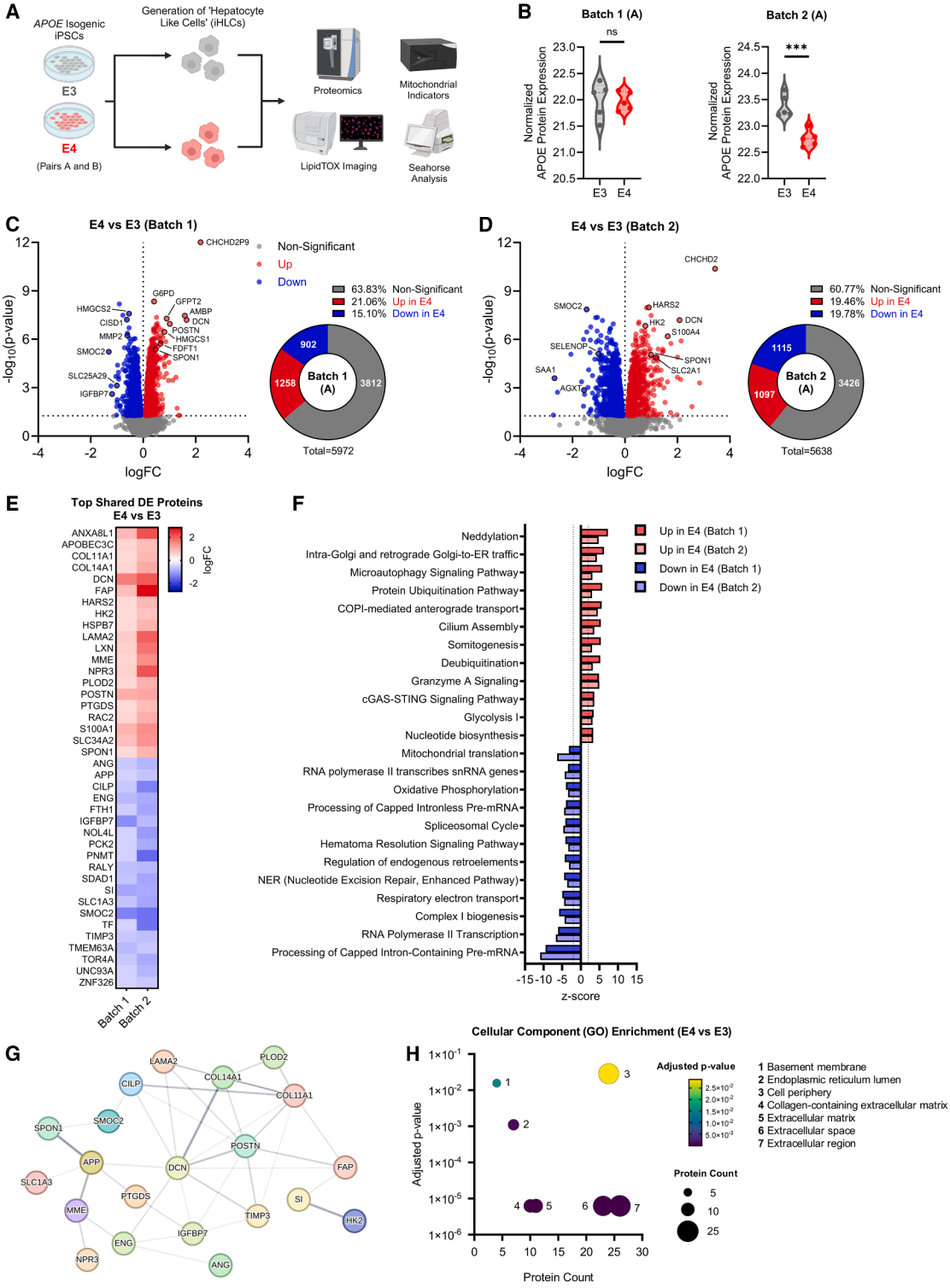

Figure 4. Proteomics analysis of *APOE* isogenic iHLCs

(A) iHLC study schematic. Two pairs of isogenic iPSCs (A and B) homozygous for either *APOE3* or *APOE4* were used to generate iHLCs and examine proteomic and bioenergetic outcomes. $n = 5$ per group for all iHLC proteomic outcomes.

(B) Violin plots of APOE protein expression between two sample batches in pair A isogenics. Statistical significance was determined by unpaired *t* test. ns, not significant, $^{***}p < 0.001$.

(C) Volcano plot showing upregulated and downregulated proteins between *APOE4* and *APOE3* iHLCs from batch 1.

(legend continued on next page)

phosphorylation, and respiratory electron transport pathways (Figure 2F). Complex I, II, III, IV, and V components also had sex-specific expression patterns between *APOE4* and *APOE3* mice (Figure 2G). Mitochondrial protein import and degradation pathways showed overall directionality differences between whole liver and isolated mitochondria proteomics in female mice (Figure 2H). Additionally, Chchd2, Mtx1, Ssbp1, and Yme1l1 were differentially expressed in whole liver and isolated mitochondria in *APOE4* vs. *APOE3* female mice (Figure 2H). Sex-dependent *APOE* genotype differences were observed in proteins that are involved in the TCA cycle and pyruvate metabolism, where females showed a downregulation of these proteins compared to males between *APOE4* and *APOE3* mice (Figure 2I). Sex differences were observed irrespective of *APOE* genotype in these mice (Figure S2). This included a decrease in proteins and pathways associated with the TCA cycle in male *APOE3* mice when compared to females (Figure S2C).

APOE genotype and sex interact to alter mitochondrial respiration in the liver

To examine functional differences in mitochondria, we leveraged Seahorse respirometry analysis in isolated liver mitochondria from *APOE*-TR mice. Fatty acid-driven state 2 and 3 respiration (PCoA) was higher in males across both genotypes (main effect of sex) (Figures 3A and 3B). We also observed a trend for increased state 2 and state 3 fatty acid-driven respiration in *APOE4* mice when compared to *APOE3* mice (Figures 3A and 3B). Fatty acid-driven state 3S and uncoupled respiration showed main effects of sex and an interaction between sex and genotype, where male *APOE4* mice had reduced uncoupled respiration (Figures 3C and 3D). There was no difference in carbohydrate-driven state 2 or 3 respiration between sex or genotype (Figures 3E and 3F). Carbohydrate-driven state 3S and uncoupled respiration showed an interaction between sex and genotype, where female *APOE4* mice had increased respiration for these states when compared to female *APOE3* mice (Figures 3G and 3H). Additionally, male *APOE3* mice exhibited increased respiration in these states compared to their female counterparts (Figures 3G and 3H).

APOE genotype drives significant changes to the proteome in iHLCs

To examine potential hepatocyte-specific effects of *APOE* genotype, we generated iPSC-derived iHLCs from two isogenic pairs of iPSCs. Characterization of these iHLCs showed expected expression of mature hepatocyte (MH) markers (Figure S3). Our primary goal was to examine proteomic and bioenergetic outcomes in these cells (Figure 4A). We carried out proteomic analysis on iHLCs generated in two batches from isogenic pair A, to control for potential variability in differentiation efficiency (Figure S3). APOE protein expression in iHLCs was the same for *APOE3* and *APOE4* cells in batch 1 but decreased in *APOE4* iHLCs in batch 2 (Figure 4B). Differences between batches are likely a consequence of higher MH protein expression in batch 1 when compared to batch 2, which may affect APOE expression patterns (Figure S3).[21] *APOE4* iHLCs from batch 1 showed 1,258 upregulated proteins (21.06%) and 902 downregulated proteins (15.10%) when compared to *APOE3* cells, while batch 2 *APOE4* iHLCs showed 1,097 upregulated proteins (19.46%) and 1,115 downregulated proteins (19.78%) (Figures 4C and 4D). Proteins that were upregulated in *APOE4* iHLCs in both batches included those associated with lipid metabolism, glycolysis, inflammation, and extracellular matrix (ECM) remodeling. In contrast, those downregulated by *APOE4* in both batches were associated with ribosomal function, cell proliferation, and regeneration (Figures 4C–4E). We also observed differential expression of proteins associated with AD. This included decreased amyloid precursor protein (APP) levels in *APOE4* iHLCs (Figure 4E). IPA analysis of pathways showed an upregulation in neddylation, Golgi/ER trafficking, autophagy, cGAS-STING, and glycolysis pathways among others in *APOE4* iHLCs (Figure 4F). Downregulated pathways in both batches included mitochondrial translation, oxidative phosphorylation, spliceosome, processing of capped intron-less pre-mRNA, nucleotide excision repair, complex I biogenesis, and transcription in *APOE4* iHLCs (Figure 4F). Due to differences associated with ECM remodeling, we next performed STRING and Gene Ontology (GO) analysis of top differentially expressed proteins from Figure 4E. Interestingly, cellular components related to the ECM were significantly enriched in *APOE4* iHLCs (Figures 4G and 4H).

APOE4 isogenic iHLCs display impaired mitochondrial function and increased glycolysis

Because of differences in mitochondrial pathways in the proteomics dataset, we next examined mitochondrial and glycolytic function in both isogenic pairs of iHLCs. *APOE4* iHLCs derived from both pair A and pair B isogenic lines had significantly reduced basal respiration, maximal proton leak, and ATP- linked respiration (Figures 5A–5D). *APOE4* iHLCs also showed reduced complex IV-driven respiration/flux in both isogenic pairs, with disparate results for complex I (reduced in group B) and complex II (increased in group A) fluxes (Figures 5E and 5F). Mitochondrial membrane potential and mitochondrial superoxide production were increased in pair A *APOE4* iHLCs but not pair B cells (Figures 5G–5I and 5L–5N). Hydrogen peroxide (H_2O_2) levels, a form of ROS, were increased in both pair A and B *APOE4* iHLCs (Figures 5J and 5O). Mitochondrial calcium (Ca^{2+}) levels were increased in pair B *APOE4* iHLCs but not pair A (Figures 5K and 5P). Increased mitochondrial membrane potential is often associated with increased ROS production.[22]

Glycolytic function was increased in both isogenic pairs of iPSC-derived *APOE4* iHLCs, including basal glycolysis and

(D) Volcano plot showing upregulated and downregulated proteins between *APOE4* and *APOE3* iHLCs from batch 2.
(E) Heatmap of the top 20 most significant upregulated and top 20 most significant downregulated proteins ($p < 0.05$) shared between batch 1 and batch 2.
(F) IPA pathway analysis showing top 12 upregulated and top 12 downregulated pathways shared in both batch 1 and 2 between *APOE4* and *APOE3* iHLCs.
(G) STRING network analysis of the most significant upregulated and downregulated proteins shared between batch 1 and batch 2 in *APOE4* vs. *APOE3* iHLCs.
(H) Cellular component Gene Ontology (GO) analysis of the top 20 upregulated and top 20 downregulated proteins in *APOE4* vs. *APOE3* iHLCs.
See also Figure S3.

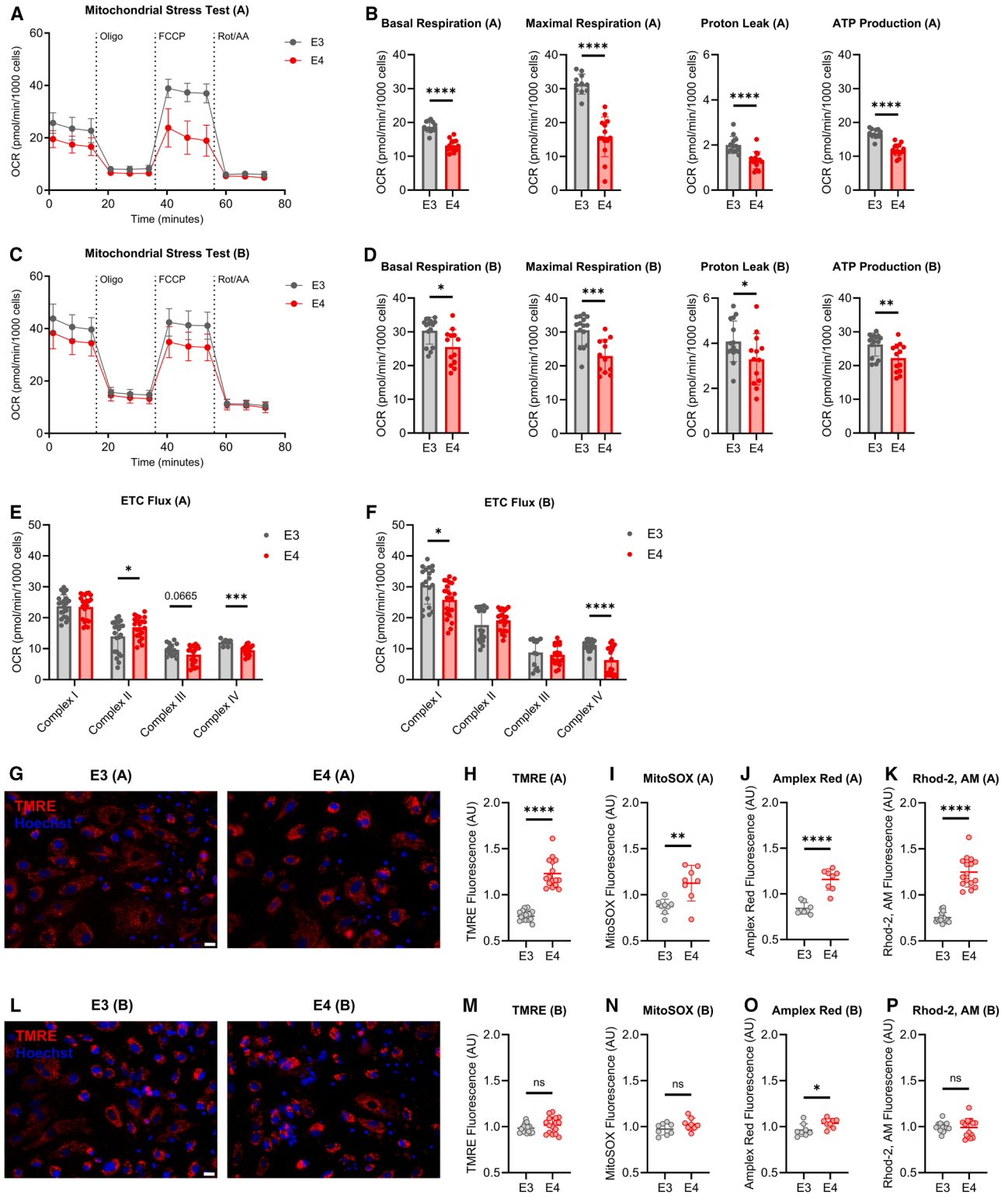

Figure 5. Mitochondrial function in *APOE* isogenic iHLCs

(A) Mitochondrial stress test (MST) tracing from isogenic pair A.

(B) Quantification of basal respiration, maximal respiration, proton leak, and ATP-production linked respiration from isogenic pair an MST. n = 13–14 per group.

(C) MST tracing from isogenic pair B.

(legend continued on next page)

glycolytic capacity (Figures 6A–6D). Based on these data, we wanted to examine glucose/pyruvate oxidation. Using UK5099, a mitochondrial pyruvate carrier (MPC) inhibitor, we found that mitochondrial pyruvate oxidation was reduced/impaired in both pairs of *APOE4* isogenic iHLCs as indicated by a smaller acute response (Figures 6E–6H).[23] Unlike *APOE3* iHLCs, *APOE4* cells treated with UK5099 also exhibited lower maximal respiration compared to untreated *APOE4* cells, suggesting an increased reliance on glucose/pyruvate metabolism (Figures 6E–6H). Unsurprisingly, glucose metabolism-associated proteins were largely upregulated in proteomic analysis (Figures 6I and 6J). This included a consistent upregulation of PGAM1 in *APOE4* isogenic iHLCs (Figure 6I).

Cholesterol and lipid metabolism are altered by APOE genotype in iHLCs

We next wanted to examine long chain fatty acid (LCFA) oxidation in these iHLCs. This was done using etomoxir (Eto), which is an inhibitor of carnitine palmitoyltransferase-1 (CPT1), a key rate-limiting step in FAO.[24] Interestingly, *APOE4* cells treated with Eto showed a reduced acute response in both isogenic pairs indicating impaired LCFA oxidation (Figures 7A–7D). Additionally, maximal respiration was lower in *APOE4* iHLCs when treated with Eto, an effect not seen in *APOE3* cells (Figures 7A–7D). This suggests *APOE4* iHLCs rely more heavily on mitochondrial oxidation of LCFAs via CPT1 during high substrate demand. Finally, we performed lipid droplet (LD) staining and found that *APOE4* iHLCs have an increased number of LDs per cell, but the size of LDs was not changed (Figures 7E–7H). The SREBF2 protein network, or sterol regulatory element-binding protein 2, which is a transcription factor critical for cholesterol homeostasis and synthesis was upregulated in *APOE4* iHLCs when compared to their *APOE3* counterparts (Figure 7I). We specifically saw an upregulation of proteins involved in fatty acid metabolism/synthesis (ACACA, ACLY, FASN, and AACS) and lipid trafficking (FABP5) which is coupled to LD formation (Figure 7I). Additional enzymes involved in the cholesterol biosynthetic pathway (HMGCS1, FDFT1, DHCR24, and SQLE) were also upregulated, suggesting coordinated activation of lipogenic and sterol synthesis pathways that may further contribute to LD expansion (Figure 7I).

Integrated liver and iHLC proteomics identifies APOE4-associated metabolic changes

To validate *APOE4*-dependent alterations in metabolism, we performed an integrated analysis of whole liver and iHLC proteomic datasets. It is important to note that we combined data from both male and female mice to capture sex-independent effects. Comparing whole livers to iHLCs identified 70 shared proteins that were differentially expressed (Figure 8A). These proteins were then analyzed using GO and Kyoto Encyclopedia of Genes and Genomes (KEGG) pathway analysis to identify processes and pathways altered by *APOE* genotype across models. Interestingly, proteins associated with monocarboxylic acid, carbohydrate, and fatty acid metabolic processes and glycolysis/gluconeogenesis were significantly enriched (Figure 8B). We next generated a heatmap of 30 proteins showing consistent directional changes across both models (Figure 8C). *APOE4* caused a consistent upregulation of key metabolic proteins, including those associated with fatty acid desaturation (CYB5A), retinoid metabolism (RDH11), glycogen synthesis and glycoprotein processing (UGP2 and MAN1A1), and stress-responsive metabolic regulation (PPM1F) in both whole livers and iHLCs. (Figure 8C). In contrast, *APOE4* consistently downregulated proteins involved in core metabolic pathways, including mitochondrial oxidative phosphorylation (NDUFA9), the TCA cycle (SUCLG2), and cholesterol and bile acid metabolism (CYP27A1) (Figure 8C). To confirm key changes observed in proteomics across all analyses, we performed western blot analysis. Consistent with our proteomic findings, we saw reduced protein levels of CYP27A1 in *APOE4* mouse livers and iHLCs and an increase in FDFT1 (Figures 8D–8G). PGAM1 was also consistent with proteomic findings with a decrease in *APOE4* mouse livers and an increase in *APOE4* iHLCs (Figures 8D–8G).

DISCUSSION

While much is known regarding the brain and *APOE* genetic variation, the impact on hepatic metabolism remains relatively understudied. Recent studies have begun to address this knowledge gap and increase our understanding of the importance *APOE* genotype may play in regulating liver metabolism.[16–18] Leveraging multiple approaches, we show that *APOE4* genotype interacts with sex differences to drive significant alterations to hepatic metabolism in the liver of young *APOE*-TR mice and isogenic iHLCs.

When measuring hepatic APOE levels, we did not observe significant differences across sex or genotype despite other studies reporting that *APOE4* reduces hepatic APOE expression.[17,25] These discrepancies may be attributed to differences in mouse age and/or strain. Furthermore, changes to liver health observed in this study may be driven by APOE function rather than differences in protein expression levels.

We explored how *APOE* genotype alters the hepatic proteome and mitochondrial function. Remarkably, *APOE4* females exhibited a significantly larger number of differentially expressed proteins compared to their *APOE3* counterparts, an effect that was less pronounced in males. This is a critical consideration

(D) Quantification of basal respiration, maximal respiration, proton leak, and ATP-production-linked respiration from isogenic pair B MST. n = 12–15 per group.
(E) Electron transport chain (ETC) flux through complex I, II, III, and IV in isogenic pair A. n = 7–22 per group.
(F) ETC flux through complex I, II, III, and IV in isogenic pair B. n = 14–22 per group.
(G) Representative tetramethyl rhodamine, ethyl ester, perchlorate (TMRE) images from isogenic pair A. Scale bars, 50 μm.
(H–K) Quantification of TMRE (H), MitoSOX (I), Amplex Red (J), and Rhod-2 AM (K) fluorescence intensities from isogenic pair A. n = 8–16 per group.
(L) Representative TMRE images from isogenic pair B. Scale bars, 50 μm.
(M–P) Quantification of TMRE (M), MitoSOX (N), Amplex Red (O), and Rhod-2 AM (P) fluorescence intensities from isogenic pair B. n = 8–16 per group. (B, D, E–F, H–K, and M–P) Statistical significance was determined by unpaired t test. Data are shown as mean ± SD. ns = not significant, $^{*}p < 0.05$, $^{**}p < 0.01$, $^{***}p < 0.001$, $^{****}p < 0.0001$.

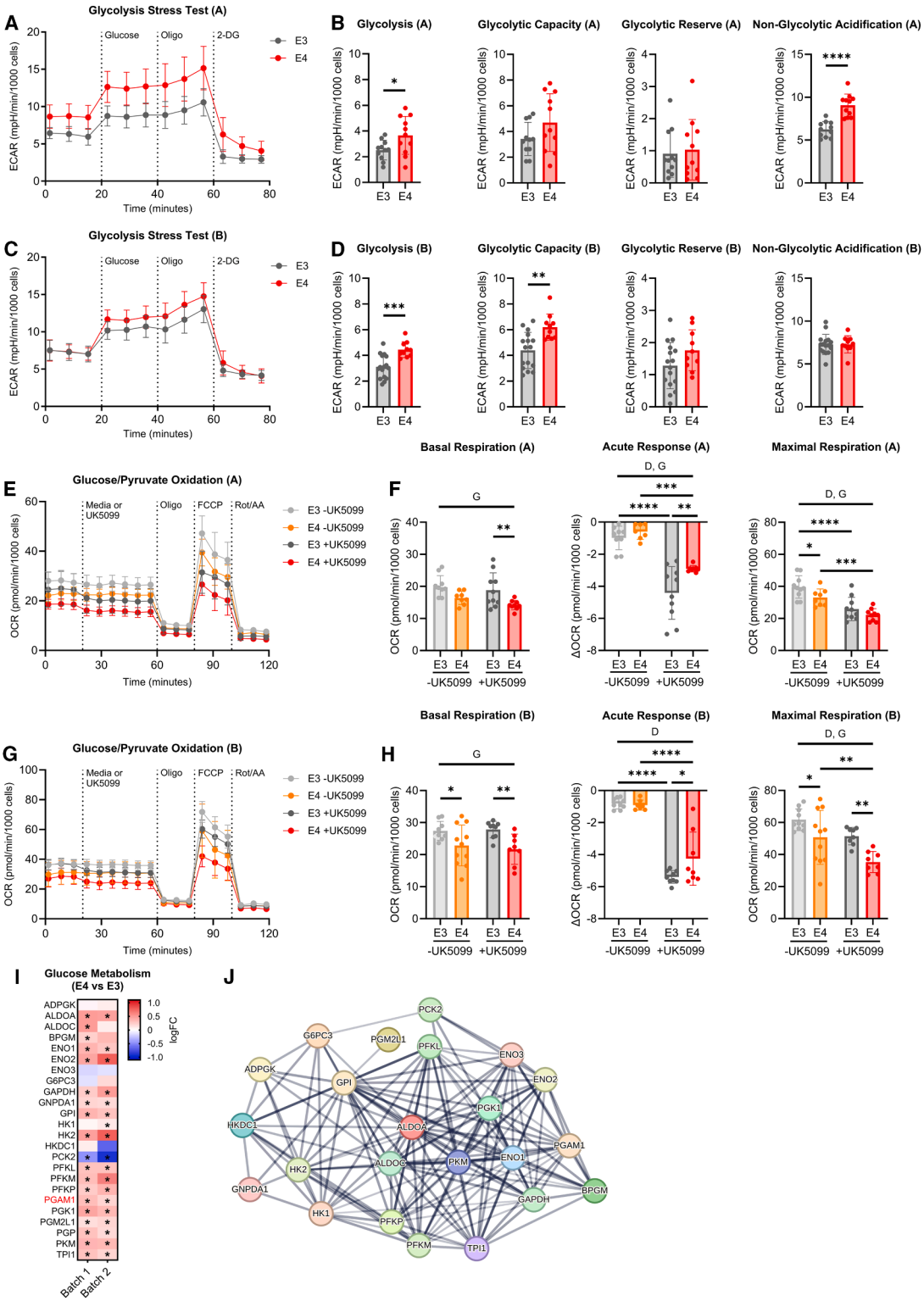

Figure 6. Glycolytic function and glucose/pyruvate oxidation in *APOE* isogenic iHLCs

(A) Glycolytic stress test (GST) tracing from isogenic pair A.

(B) Quantification of basal glycolysis, glycolytic capacity, glycolytic reserve, and non-glycolytic acidification from isogenic pair A GST. n = 11 per group.

(C) GST tracing from isogenic pair B.

(D) Quantification of basal glycolysis, glycolytic capacity, glycolytic reserve, and non-glycolytic acidification from isogenic pair B GST. n = 10–16 per group.

(legend continued on next page)

since women with at least one *APOE4* allele are at a higher risk of developing AD than men.[26,27] Analysis of altered pathways in the entire liver revealed a genotype-by-sex interaction. Specifically, *APOE4* females exhibited an upregulation of the electron transport chain (ETC) and oxidative phosphorylation when compared to *APOE3* females, whereas *APOE4* males showed a downregulation of these pathways. These changes were relatively consistent with functional respiratory data, where *APOE4* females exhibited increased respiration across multiple respiratory states compared to *APOE3* females.

Examining differences between sexes revealed that *APOE3* male mice had an upregulation of not only oxidative phosphorylation, but peroxisomal lipid metabolism as well when compared to females. An upregulation of lipid metabolism at peroxisomes may explain increased lipid-driven respiration in *APOE3* male mice. This is supported by past research showing peroxisome and mitochondrial lipid metabolism is coupled.[28–30] While we performed respiration on isolated mitochondria, this increase in peroxisomal lipid metabolism may have primed mitochondria in male mice. Finally, acetyl-CoA acetyltransferase 2 (Acat2), a protein involved in the biosynthesis of cholesterol, is downregulated in *APOE4* female and male mice. Past research has shown that ablation of *Acat2* leads to increased plasma triglycerides and can cause mice on a high-fat diet to become more susceptible to insulin resistance, while *Acat2* overexpression promotes cholesterol metabolism and reduces blood glucose levels.[31–34]

In addition to changes in mitochondrial energy and lipid metabolism, we also observed decreased glycolysis in *APOE4* females when compared to their *APOE3* counterparts. This is a notable finding as the liver plays a major role in whole body glucose metabolism.[35] Interestingly, a downregulation of Rap1 signaling in *APOE4* versus *APOE3* male mice was observed. Numerous studies have shown that an upregulation of Rap1 signaling can protect the liver from hepatic steatosis and it is also implicated in glucose metabolism/signaling.[36,37] Sex-specific differences were also observed in the TCA cycle, with *APOE4* female mice exhibiting a downregulation of this pathway, while *APOE4* male mice showed an upregulation compared to their *APOE3* counterparts. This is interesting because state 3S respiration (succinate-driven) is increased in *APOE4* female mice, an effect not seen in *APOE4* males. Sex comparisons revealed that *APOE3* male mice had a decrease in the TCA cycle when compared to their female counterparts. This may indicate increased enzymatic activity since *APOE3* males had higher pyruvate/malate-driven respiration though this requires further investigation into succinate dehydrogenase activity.

We also examined proteins involved in mitochondrial import between whole liver and isolated mitochondria in female mice. Specifically, there was an upregulation of the mitochondrial protein import pathway (Timm and Tomm machinery) in the livers of *APOE4* female mice. However, when we examine isolated mitochondria, we saw the opposite. This discrepancy could indicate several possibilities, including impaired import of mitochondrial proteins, selection of mitochondria less efficient at protein import during isolation, or potential compensation in *APOE4* female mice.

In this study, we found that *APOE4* caused an upregulation of proteins and pathways associated with inflammatory and immune signaling. Mechanisms of this outcome are not known; however, prior studies have implicated that metabolic stress can act as a potent inflammatory activator for hepatic stellate cells within the liver.[38] Future studies should work to clarify these findings to understand how *APOE4* modulates immune function within the liver and compare these to effects observed within the brain as *APOE4* is known to modulate neuroinflammation and glial cell function.[39]

Differences between male and female mice suggest significant differential effects of *APOE* genotype in relation to sex. In humans, *APOE* genotype interacts with sex to modulate AD risk, but the role liver metabolism contributes to this is not known.[27] It is established that women have a higher risk of steatosis post menopause compared to age-matched men while prior to menopause women are protected.[40] Women also have a higher risk for AD overall than men.[41] Potential reasons for sex differences include sex hormone effects, such as estrogen or progesterone, sex chromosome differences, and overall metabolic differences. While mechanisms are not known for sex differences in the effects of *APOE* genotype understanding, these phenotypes in liver is imperative to understand the roles metabolism may contribute.

APOE isogenic iHLCs were used to examine hepatocyte-specific changes that were void of non-parenchymal cells that were in the livers of mice. Several upregulated proteins in *APOE4* iHLCs have been previously linked to AD and ECM remodeling.[19,42–49] This includes proteins such as membrane metalloendopeptidase or neprilysin (MME), decorin (DCN), and F-spondin/spondin-1 (SPON1). Notable, proteins decreased in *APOE4* iHLCs included APP, ferritin heavy chain 1 (FTH1), insulin-like growth factor binding protein 7 (IGFBP7), SPARC-related modular calcium binding 2 (SMOC2), and metalloproteinase inhibitor 3 (TIMP3). One of the studies mentioned above specifically investigated *APOE4*-dependent changes in serum proteomics from AD patients and found an increase in SPON1.[19] However, this change was independent of *APOE* genotype. Similar to our findings, they also observed alterations to ECM proteins. This is notable as ECM proteins play a critical role in liver fibrosis.[50,51]

(E) Glucose/pyruvate oxidation stress test from isogenic pair A.
(F) Quantification of basal respiration, acute response, and maximal respiration from isogenic pair A glucose/pyruvate oxidation stress test. n = 7–10 per group.
(G) Glucose/pyruvate oxidation stress test from isogenic pair B.
(H) Quantification of basal respiration, acute response, and maximal respiration from isogenic pair B glucose/pyruvate oxidation stress test. n = 7–11 per group.
(I) Significant DE proteins involved in glucose metabolism pathway from IPA.
(J) Glucose metabolism protein network from STRING analysis.
(B and D) Statistical significance was determined by unpaired t test and (F and H) two-way ANOVA with Fisher's LSD post hoc. Data are shown as mean ± SD. $^{*}p < 0.05$, $^{**}p < 0.01$, $^{***}p < 0.001$, $^{****}p < 0.0001$. D, drug, G, genotype.

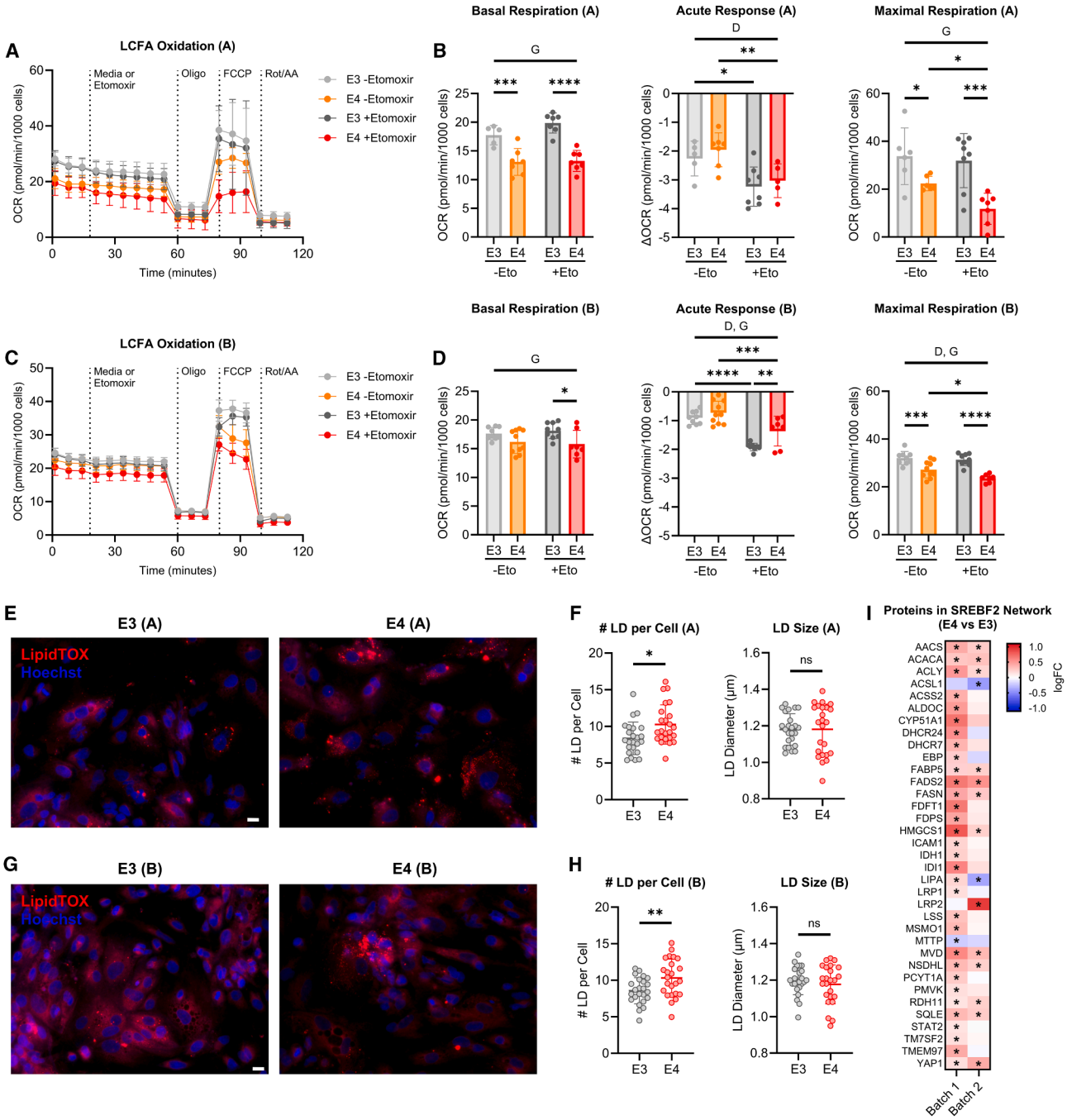

Figure 7. Fatty acid oxidation and LipidTOX staining in *APOE* isogenic iHLCs

(A) Long chain fatty acid (LCFA) oxidation stress test from isogenic pair A.

(B) Quantification of basal respiration, acute response, and maximal respiration from isogenic pair An LCFA oxidation stress test. n = 6–8 per group.

(C) LCFA oxidation stress test from isogenic pair B.

(D) Quantification of basal respiration, acute response, and maximal respiration from isogenic pair B LCFA oxidation stress test. n = 7–10 per group.

(E) Representative LipidTOX images from isogenic pair A. Scale bars, 50 µm.

(F) Quantification of lipid droplet (LD) numbers per cell and diameter (µm) from isogenic pair A. n = 24 per group.

(G) Representative LipidTOX images from isogenic pair B. Scale bars, 50 µm.

(H) Quantification of LD numbers per cell and diameter (µm) from isogenic pair B. n = 24 per group.

(I) Comparison analysis showing significantly altered proteins in SREBF2 network from proteomics.

(B and D) Statistical significance was determined by a two-way ANOVA with Fisher's LSD post hoc and (F and H) unpaired t test. Data are shown as mean ± SD. ns = not significant, $^{*}p < 0.05$, $^{**}p < 0.01$, $^{***}p < 0.001$, $^{****}p < 0.0001$. D, drug, G, genotype.

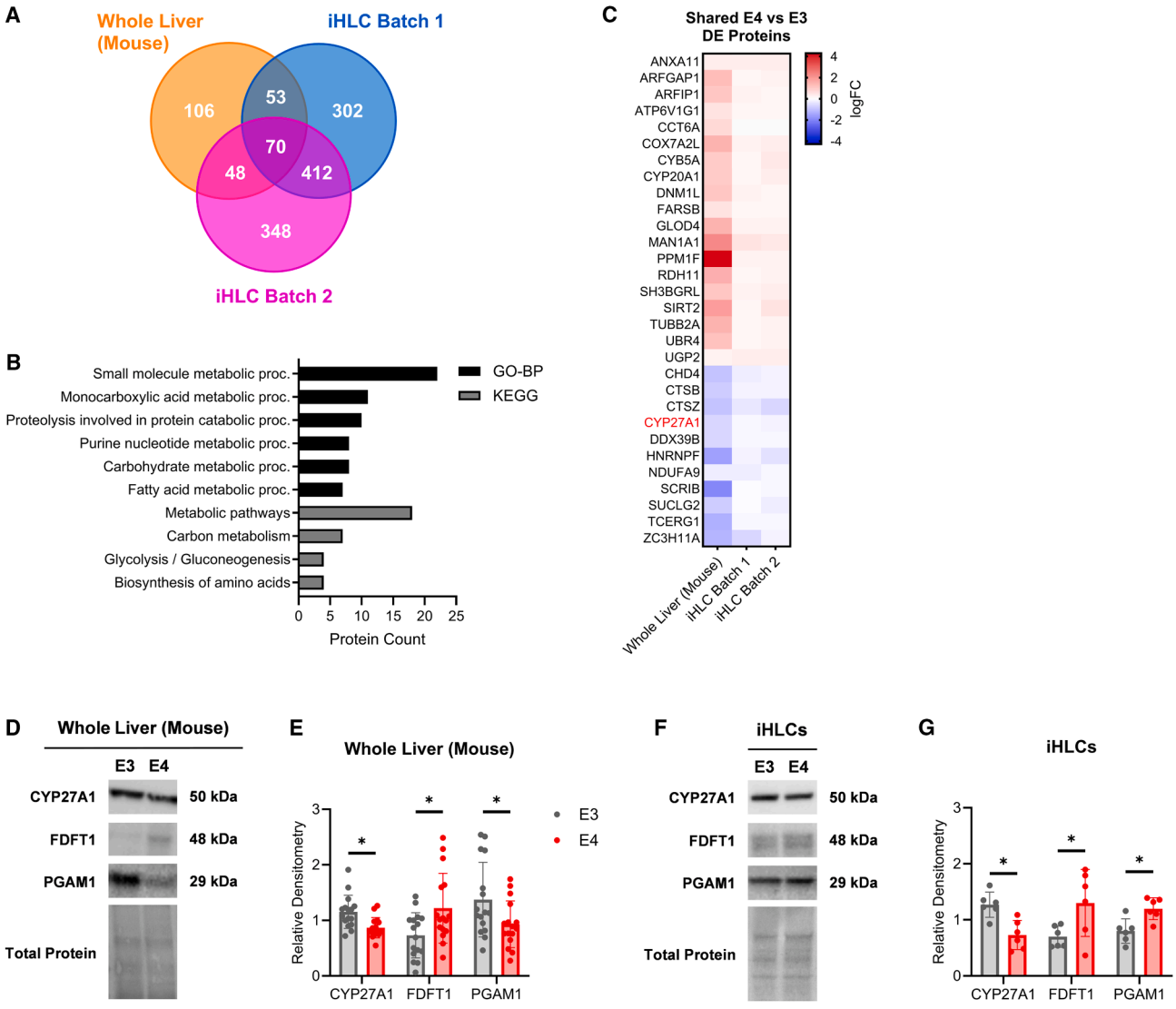

Figure 8. Comparative proteomic analysis of whole mouse livers and iHLCs

(A) Venn diagram depicting overlap of significant DE proteins in *APOE4* vs. *APOE3* across whole mouse livers and iHLCs (batch 1 and 2).

(B) Gene Ontology Biological Process (GO-BP) and KEGG pathway analysis of the 70 proteins shared across mouse liver and iHLCs, showing protein counts per category.

(C) Heatmap of proteins consistently upregulated or downregulated in *APOE4* vs. *APOE3* across whole mouse liver and iHLCs (batch 1 and 2).

(D–E) Western blot analysis of CYP27A1, FDFT1, and PGAM1 in *APOE4* and *APOE3* whole mouse livers, with relative densitometry quantification. $n = 16$ per group.

(F–G) Western blot analysis of CYP27A1, FDFT1, and PGAM1 in *APOE4* and *APOE3* isogenic iHLCs, with relative densitometry quantification. $n = 6$ per group.

(E and G) Statistical significance was determined by unpaired *t* test. Data are shown as mean ± SD. $^{*}p < 0.05$.

Proteins and pathways associated with metabolism were altered in *APOE4* iHLCs. This included a downregulation of pathways related to mitochondrial function. These data is further supported by decreased mitochondrial respiration and ETC function in *APOE4* iHLCs. Unsurprisingly, *APOE4* iHLCs had increased H_2O_2 levels, and an upregulation of pathways known to be associated with mitochondrial stress such as cGAS-STING signaling.[52] There was also an upregulation of glycolysis and associated proteins including hexokinase 2 (HK2) and SLC2A1 (glucose transporter type 1 or GLUT1) in *APOE4* cells. Glycolytic function was increased in *APOE4* iHLCs, reflecting the elevated demand for glucose and pyruvate as fuel substrates. This is an interesting finding as there was a decrease in proteins and pathways associated with glycolysis/glucose metabolism in the livers of mice. This difference may be explained by the fact that iHLCs are isolated cells, in contrast to whole tissue, which contains numerous cell types with potentially different signaling dynamics. Irrespective of this, past studies have shown that *APOE* genotype can modulate glycolysis and glucose metabolism.[53–55] Additionally, *APOE4* iHLCs have increased demand

for fatty acids and LD accumulation indicating altered lipid homeostasis. Looking further at proteomics, we found that proteins in the SREBF2 network are upregulated indicating increased cholesterol and fatty acid synthesis.[56] Taken together, these results indicate that *APOE4* iHLCs exhibit dysregulated lipid metabolism, characterized by both altered lipid storage and increased reliance on lipid substrates (particularly, fatty acids) for energy production.

We also found that proteins associated with cholesterol metabolism were differentially expressed across all comparisons. This includes an increase of farnesyl-diphosphate farnesyltransferase 1 (FDFT1) in *APOE4* versus *APOE3* mice and iHLCs. FDFT1 is involved in the mevalonate pathway and has been shown to be previously modified by *APOE* genotype in various CNS cell types.[57,58] On the other hand, CYP27A1, which is responsible for the conversion of cholesterol into bile acids is consistently down in both models. An upregulation of FDFT1 indicates increased cholesterol synthesis, while the downregulation of CYP27A1 implies reduced cholesterol clearance via bile acid formation. These data, combined with an increase in fatty acid synthesis proteins and the formation of LDs in *APOE4* iHLCs, suggests a shift toward enhanced cholesterol and lipid accumulation.

In conclusion, this study demonstrates that *APOE* genetic variation significantly impacts markers of hepatic glucose and lipid metabolism, as well as mitochondrial function. These findings raise additional questions, including the role of liver metabolism and health in contributing to AD risk and onset. This highlights the need for follow-up studies to validate and expand upon these results.

Limitations of the study

While this study provides new insights into *APOE* genotype-dependent changes in hepatic metabolism, several limitations should be considered. First, we did not include female isogenic iHLCs, which would be valuable for examining sex-specific hepatocyte effects. Moreover, iHLCs, while valuable, are not fully mature and differences in metabolism and protein expression may be influenced by this. Another important limitation is that some metabolic pathways, such as glycolysis, were regulated in opposite directions in *APOE4* mouse livers versus iHLCs, reflecting model-specific differences and extrapolation of these findings to human liver metabolism should be done cautiously. This study was completed in relatively young mice (4 months of age) and may limit some findings that could be present at older ages. However, the significant phenotypes observed at this young age implicate that *APOE* genotype effects on metabolism might occur early on. The current study focused on liver and hepatocyte effects and did not examine brain specific changes. Future studies are currently examining whole brain and brain cell type-specific changes with respect to *APOE* genotype. The impact of *APOE* genotype is also not limited to *APOE3* and *APOE4* homozygosity, as these do not represent the full range of allelic combinations found in the population. Future studies may benefit from examining the *APOE2* allele in relation to hepatic health.

RESOURCE AVAILABILITY

Lead contact

Requests for further information, resources, and data should be directed to and will be fulfilled by the lead contact, Heather M. Wilkins (hwilkins@kumc.edu).

Materials availability

This study did not generate new unique reagents.

Data and code availability

- Data are available through Mendeley "APOE4 drives widespread changes to the hepatic proteome and alters metabolic function" iScience," Mendeley Data, v.1, https://doi.org/10.17632/yzh2nz7xyy.1, and proteomics data are available through MassIVE repository code MSV000100053.
- No code was used in this study.

ACKNOWLEDGMENTS

This study was supported by the Margaret "Peg" McLaughlin and Lydia A. Walker Opportunity Fund, the University of Kansas Alzheimer's Disease Center P30AG072973 (to H.M.W., J.K.M., and J.P.T.), Kansas Center for Metabolism and Obesity Research Center P20 GM144269 (to J.P.T.), R01AG078186, R00AG056600, and Alzheimer's Association grant 23AARG-1023294 (to H.M.W.), R01DK121497 Supplement, R01AG069781, and VA Merit Review grant 1I01BX002567 (to J.P.T.), T32HD057850 (to V.C.), T32AG078114 (to C.R.L. and C.N.J.), and T32DK128770 (to E.F.), IDeA National Resource for Quantitative Proteomics, and NIH/NIGMS grant R24GM137786. The content is solely the responsibility of the authors and does not necessarily represent the official views of the National Institutes of Health.

AUTHOR CONTRIBUTIONS

Acquisition of funding, H.M.W. and J.K.M.; project conceptualization, C.R.L. and H.M.W.; investigation, C.R.L., C.N.J., V.C., E.F., M.B., A.L.T., and H.M.W.; resources, J.P.T., P.C.G., J.K.M., and H.M.W.; methodology, C.R.L., J.P.T., and H.M.W.; supervision, H.M.W.; writing – original draft preparation, C.R.L. and H.M.W.; writing – review and editing, all authors.

DECLARATION OF INTERESTS

The authors declare no competing interests.

STAR★METHODS

Detailed methods are provided in the online version of this paper and include the following:

- KEY RESOURCES TABLE
- EXPERIMENTAL MODEL AND STUDY PARTICIPANT DETAILS
  - Animals
  - Human induced pluripotent stem cell culture
- METHOD DETAILS
  - Generation of hepatocyte-like cells
  - Mitochondrial isolation from whole liver
  - Proteomics
  - APOE enzyme-linked immunosorbent assay (ELISA)
  - Western blotting
  - Immunocytochemistry (ICC)
  - Isolated mitochondria respiration
  - Cellular respiration
  - LipidTOX imaging and quantification
  - Mitochondrial indicator assays
- QUANTIFICATION AND STATISTICAL ANALYSIS
  - Proteomic data analysis

- Statistical analysis

SUPPLEMENTAL INFORMATION

Supplemental information can be found online at https://doi.org/10.1016/j.isci.2026.115035.

Received: August 20, 2025
Revised: September 9, 2025
Accepted: January 28, 2026
Published: February 17, 2026

REFERENCES

1. Holtzman, D.M., Herz, J., and Bu, G. (2012). Apolipoprotein E and apolipoprotein E receptors: normal biology and roles in Alzheimer disease. Cold Spring Harb. Perspect. Med. *2*, a006312. https://doi.org/10.1101/cshperspect.a006312.
2. Yamazaki, Y., Zhao, N., Caulfield, T.R., Liu, C.C., and Bu, G. (2019). Apolipoprotein E and Alzheimer disease: pathobiology and targeting strategies. Nat. Rev. Neurol. *15*, 501–518. https://doi.org/10.1038/s41582-019-0228-7.
3. Hatters, D.M., Peters-Libeu, C.A., and Weisgraber, K.H. (2006). Apolipoprotein E structure: insights into function. Trends Biochem. Sci. *31*, 445–454. https://doi.org/10.1016/j.tibs.2006.06.008.
4. Frieden, C., Wang, H., and Ho, C.M.W. (2017). A mechanism for lipid binding to apoE and the role of intrinsically disordered regions coupled to domain-domain interactions. Proc. Natl. Acad. Sci. USA *114*, 6292–6297. https://doi.org/10.1073/pnas.1705080114.
5. Narasimhan, S., Holtzman, D.M., Apostolova, L.G., Cruchaga, C., Masters, C.L., Hardy, J., Villemagne, V.L., Bell, J., Cho, M., and Hampel, H. (2024). Apolipoprotein E in Alzheimer's disease trajectories and the next-generation clinical care pathway. Nat. Neurosci. *27*, 1236–1252. https://doi.org/10.1038/s41593-024-01669-5.
6. Liu, M., Kuhel, D.G., Shen, L., Hui, D.Y., and Woods, S.C. (2012). Apolipoprotein E does not cross the blood-cerebrospinal fluid barrier, as revealed by an improved technique for sampling CSF from mice. Am. J. Physiol. Regul. Integr. Comp. Physiol. *303*, R903–R908. https://doi.org/10.1152/ajpregu.00219.2012.
7. Chernick, D., Ortiz-Valle, S., Jeong, A., Qu, W., and Li, L. (2019). Peripheral versus central nervous system APOE in Alzheimer's disease: Interplay across the blood-brain barrier. Neurosci. Lett. *708*, 134306. https://doi.org/10.1016/j.neulet.2019.134306.
8. Martinez-Martinez, A.B., Torres-Perez, E., Devanney, N., Del Moral, R., Johnson, L.A., and Arbones-Mainar, J.M. (2020). Beyond the CNS: The many peripheral roles of APOE. Neurobiol. Dis. *138*, 104809. https://doi.org/10.1016/j.nbd.2020.104809.
9. Hamilton, R.L., Wong, J.S., Guo, L.S., Krisans, S., and Havel, R.J. (1990). Apolipoprotein E localization in rat hepatocytes by immunogold labeling of cryothin sections. J. Lipid Res. *31*, 1589–1603.
10. Getz, G.S., and Reardon, C.A. (2009). Apoprotein E as a lipid transport and signaling protein in the blood, liver, and artery wall. J. Lipid Res. *50*, S156–S161. https://doi.org/10.1194/jlr.R800058-JLR200.
11. Troutwine, B.R., Hamid, L., Lysaker, C.R., Strope, T.A., and Wilkins, H.M. (2022). Apolipoprotein E and Alzheimer's disease. Acta Pharm. Sin. B *12*, 496–510. https://doi.org/10.1016/j.apsb.2021.10.002.
12. Lohmann, C., Schäfer, N., von Lukowicz, T., Sokrates Stein, M.A., Borén, J., Rütti, S., Wahli, W., Donath, M.Y., Lüscher, T.F., and Matter, C.M. (2009). Atherosclerotic mice exhibit systemic inflammation in periadventitial and visceral adipose tissue, liver, and pancreatic islets. Atherosclerosis *207*, 360–367. https://doi.org/10.1016/j.atherosclerosis.2009.05.004.
13. Wagner, T., Bartelt, A., Schlein, C., and Heeren, J. (2015). Genetic Dissection of Tissue-Specific Apolipoprotein E Function for Hypercholesterolemia and Diet-Induced Obesity. PLoS One *10*, e0145102. https://doi.org/10.1371/journal.pone.0145102.
14. Schierwagen, R., Maybüchen, L., Zimmer, S., Hittatiya, K., Bäck, C., Klein, S., Uschner, F.E., Reul, W., Boor, P., Nickenig, G., et al. (2015). Seven weeks of Western diet in apolipoprotein-E-deficient mice induce metabolic syndrome and non-alcoholic steatohepatitis with liver fibrosis. Sci. Rep. *5*, 12931. https://doi.org/10.1038/srep12931.
15. Suski, M., Olszanecki, R., Madej, J., Totoń-Żurańska, J., Niepsuj, A., Jawień, J., Bujak-Giżycka, B., Okoń, K., and Korbut, R. (2011). Proteomic analysis of changes in protein expression in liver mitochondria in apoE knockout mice. J. Proteomics *74*, 887–893. https://doi.org/10.1016/j.jprot.2011.03.003.
16. Dose, J., Nebel, A., Piegholdt, S., Rimbach, G., and Huebbe, P. (2016). Influence of the APOE genotype on hepatic stress response: Studies in APOE targeted replacement mice and human liver cells. Free Radic. Biol. Med. *96*, 264–272. https://doi.org/10.1016/j.freeradbiomed.2016.04.031.
17. Huebbe, P., Bilke, S., Rueter, J., Schloesser, A., Campbel, G., Glüer, C.C., Lucius, R., Röcken, C., Tholey, A., and Rimbach, G. (2024). Human APOE4 Protects High-Fat and High-Sucrose Diet Fed Targeted Replacement Mice against Fatty Liver Disease Compared to APOE3. Aging Dis. *15*, 259–281. https://doi.org/10.14336/AD.2023.0530.
18. Almeida, F.C., Patra, K., Giannisis, A., Niesnerova, A., Nandakumar, R., Ellis, E., Oliveira, T.G., and Nielsen, H.M. (2024). APOE genotype dictates lipidomic signatures in primary human hepatocytes. J. Lipid Res. *65*, 100498. https://doi.org/10.1016/j.jlr.2024.100498.
19. Frick, E.A., Emilsson, V., Jonmundsson, T., Steindorsdottir, A.E., Johnson, E.C.B., Puerta, R., Dammer, E.B., Shantaraman, A., Cano, A., Boada, M., et al. (2024). Serum proteomics reveal APOE-epsilon4-dependent and APOE-epsilon4-independent protein signatures in Alzheimer's disease. Nat. Aging *4*, 1446–1464. https://doi.org/10.1038/s43587-024-00693-1.
20. Rath, S., Sharma, R., Gupta, R., Ast, T., Chan, C., Durham, T.J., Goodman, R.P., Grabarek, Z., Haas, M.E., Hung, W.H.W., et al. (2021). MitoCarta3.0: an updated mitochondrial proteome now with sub-organelle localization and pathway annotations. Nucleic Acids Res. *49*, D1541–D1547. https://doi.org/10.1093/nar/gkaa1011.
21. Krumm, J., Sekine, K., Samaras, P., Brazovskaja, A., Breunig, M., Yasui, R., Kleger, A., Taniguchi, H., Wilhelm, M., Treutlein, B., et al. (2022). High temporal resolution proteome and phosphoproteome profiling of stem cell-derived hepatocyte development. Cell Rep. *38*, 110604. https://doi.org/10.1016/j.celrep.2022.110604.
22. Ahmed Selim, N., and Wojtovich, A.P. (2025). Mitochondrial membrane potential and compartmentalized signaling: Calcium, ROS, and beyond. Redox Biol. *86*, 103859. https://doi.org/10.1016/j.redox.2025.103859.
23. Yang, C., Ko, B., Hensley, C.T., Jiang, L., Wasti, A.T., Kim, J., Sudderth, J., Calvaruso, M.A., Lumata, L., Mitsche, M., et al. (2014). Glutamine oxidation maintains the TCA cycle and cell survival during impaired mitochondrial pyruvate transport. Mol. Cell *56*, 414–424. https://doi.org/10.1016/j.molcel.2014.09.025.
24. O'Connor, R.S., Guo, L., Ghassemi, S., Snyder, N.W., Worth, A.J., Weng, L., Kam, Y., Philipson, B., Trefely, S., Nunez-Cruz, S., et al. (2018). The CPT1a inhibitor, etomoxir induces severe oxidative stress at commonly used concentrations. Sci. Rep. *8*, 6289. https://doi.org/10.1038/s41598-018-24676-6.
25. Ong, Q.R., Chan, E.S., Lim, M.L., and Wong, B.S. (2014). Expression of human apolipoprotein E4 reduces insulin-receptor substrate 1 expression and Akt phosphorylation in the ageing liver. FEBS Open Bio *4*, 260–265. https://doi.org/10.1016/j.fob.2014.02.011.
26. Fleisher, A., Grundman, M., Jack, C.R., Jr., Petersen, R.C., Taylor, C., Kim, H.T., Schiller, D.H.B., Bagwell, V., Sencakova, D., Weiner, M.F., et al. (2005). Sex, apolipoprotein E epsilon 4 status, and hippocampal volume in mild cognitive impairment. Arch. Neurol. *62*, 953–957. https://doi.org/10.1001/archneur.62.6.953.
27. Altmann, A., Tian, L., Henderson, V.W., Greicius, M.D., and Alzheimer's Disease Neuroimaging Initiative Investigators. (2014). Sex modifies the

APOE-related risk of developing Alzheimer disease. Ann. Neurol. *75*, 563–573. https://doi.org/10.1002/ana.24135.

28. Park, H., He, A., Tan, M., Johnson, J.M., Dean, J.M., Pietka, T.A., Chen, Y., Zhang, X., Hsu, F.F., Razani, B., et al. (2019). Peroxisome-derived lipids regulate adipose thermogenesis by mediating cold-induced mitochondrial fission. J. Clin. Investig. *129*, 694–711. https://doi.org/10.1172/JCI120606.
29. Houten, S.M., Wanders, R.J.A., and Ranea-Robles, P. (2020). Metabolic interactions between peroxisomes and mitochondria with a special focus on acylcarnitine metabolism. Biochim. Biophys. Acta. Mol. Basis Dis. *1866*, 165720. https://doi.org/10.1016/j.bbadis.2020.165720.
30. Hu, D., Tan, M., Lu, D., Kleiboeker, B., Liu, X., Park, H., Kravitz, A.V., Shoghi, K.I., Tseng, Y.H., Razani, B., et al. (2023). TMEM135 links peroxisomes to the regulation of brown fat mitochondrial fission and energy homeostasis. Nat. Commun. *14*, 6099. https://doi.org/10.1038/s41467-023-41849-8.
31. Brown, J.M., Bell, T.A., 3rd, Alger, H.M., Sawyer, J.K., Smith, T.L., Kelley, K., Shah, R., Wilson, M.D., Davis, M.A., Lee, R.G., et al. (2008). Targeted depletion of hepatic ACAT2-driven cholesterol esterification reveals a non-biliary route for fecal neutral sterol loss. J. Biol. Chem. *283*, 10522–10534. https://doi.org/10.1074/jbc.M707659200.
32. Ma, Z., Huang, Z., Zhang, C., Liu, X., Zhang, J., Shu, H., Ma, Y., Liu, Z., Feng, Y., Chen, X., et al. (2023). Hepatic Acat2 overexpression promotes systemic cholesterol metabolism and adipose lipid metabolism in mice. Diabetologia *66*, 390–405. https://doi.org/10.1007/s00125-022-05829-9.
33. Wang, Y.J., Bian, Y., Luo, J., Lu, M., Xiong, Y., Guo, S.Y., Yin, H.Y., Lin, X., Li, Q., Chang, C.C.Y., et al. (2017). Cholesterol and fatty acids regulate cysteine ubiquitylation of ACAT2 through competitive oxidation. Nat. Cell Biol. *19*, 808–819. https://doi.org/10.1038/ncb3551.
34. Zhang, J., Kelley, K.L., Marshall, S.M., Davis, M.A., Wilson, M.D., Sawyer, J.K., Farese, R.V., Jr., Brown, J.M., and Rudel, L.L. (2012). Tissue-specific knockouts of ACAT2 reveal that intestinal depletion is sufficient to prevent diet-induced cholesterol accumulation in the liver and blood. J. Lipid Res. *53*, 1144–1152. https://doi.org/10.1194/jlr.M024356.
35. Han, H.S., Kang, G., Kim, J.S., Choi, B.H., and Koo, S.H. (2016). Regulation of glucose metabolism from a liver-centric perspective. Exp. Mol. Med. *48*, e218. https://doi.org/10.1038/emm.2015.122.
36. Martinez, P., Gomez-Lopez, G., Garcia, F., Mercken, E., Mitchell, S., Flores, J.M., de Cabo, R., and Blasco, M.A. (2013). RAP1 protects from obesity through its extratelomeric role regulating gene expression. Cell Rep. *3*, 2059–2074. https://doi.org/10.1016/j.celrep.2013.05.030.
37. Wang, Y., Spolitu, S., Zadroga, J.A., Sarecha, A.K., and Ozcan, L. (2022). Hepatocyte Rap1a contributes to obesity- and statin-associated hyperglycemia. Cell Rep. *40*, 111259. https://doi.org/10.1016/j.celrep.2022.111259.
38. Kisseleva, T., Ganguly, S., Murad, R., Wang, A., and Brenner, D.A. (2025). Regulation of Hepatic Stellate Cell Phenotypes in Metabolic Dysfunction-Associated Steatohepatitis. Gastroenterology *169*, 797–812. https://doi.org/10.1053/j.gastro.2025.03.010.
39. Parhizkar, S., and Holtzman, D.M. (2022). APOE mediated neuroinflammation and neurodegeneration in Alzheimer's disease. Semin. Immunol. *59*, 101594. https://doi.org/10.1016/j.smim.2022.101594.
40. Polyzos, S.A., and Goulis, D.G. (2024). Menopause and metabolic dysfunction-associated steatotic liver disease. Maturitas *186*, 108024. https://doi.org/10.1016/j.maturitas.2024.108024.
41. O'Neal, M.A. (2023). Women and the risk of Alzheimer's disease. Front. Glob. Womens Health *4*, 1324522. https://doi.org/10.3389/fgwh.2023.1324522.
42. Majernikova, N., Marmolejo-Garza, A., Salinas, C.S., Luu, M.D.A., Zhang, Y., Trombetta-Lima, M., Tomin, T., Birner-Gruenberger, R., Lehtonen, S., Koistinaho, J., et al. (2024). The link between amyloid beta and ferroptosis pathway in Alzheimer's disease progression. Cell Death Dis. *15*, 782. https://doi.org/10.1038/s41419-024-07152-0.
43. Wan, T., and Wang, C. (2025). SMOC2 promotes microglia activity and neuroinflammation in Alzheimer's disease. J. Alzheimers Dis. *103*, 941–950. https://doi.org/10.1177/13872877241307337.
44. Agbemenyah, H.Y., Agis-Balboa, R.C., Burkhardt, S., Delalle, I., and Fischer, A. (2014). Insulin growth factor binding protein 7 is a novel target to treat dementia. Neurobiol. Dis. *62*, 135–143. https://doi.org/10.1016/j.nbd.2013.09.011.
45. Sun, Y., Xu, S., Jiang, M., Liu, X., Yang, L., Bai, Z., and Yang, Q. (2021). Role of the Extracellular Matrix in Alzheimer's Disease. Front. Aging Neurosci. *13*, 707466. https://doi.org/10.3389/fnagi.2021.707466.
46. Jiang, R., Smailovic, U., Haytural, H., Tijms, B.M., Li, H., Haret, R.M., Shevchenko, G., Chen, G., Abelein, A., Gobom, J., et al. (2022). Increased CSF-decorin predicts brain pathological changes driven by Alzheimer's Abeta amyloidosis. Acta Neuropathol. Commun. *10*, 96. https://doi.org/10.1186/s40478-022-01398-5.
47. Park, J.H., Cho, S.J., Jo, C., Park, M.H., Han, C., Kim, E.J., Huh, G.Y., and Koh, Y.H. (2022). Altered TIMP-3 Levels in the Cerebrospinal Fluid and Plasma of Patients with Alzheimer's Disease. J. Pers. Med. *12*, 827. https://doi.org/10.3390/jpm12050827.
48. Hoe, H.S., Cooper, M.J., Burns, M.P., Lewis, P.A., van der Brug, M., Chakraborty, G., Cartagena, C.M., Pak, D.T.S., Cookson, M.R., and Rebeck, G.W. (2007). The metalloprotease inhibitor TIMP-3 regulates amyloid precursor protein and apolipoprotein E receptor proteolysis. J. Neurosci. *27*, 10895–10905. https://doi.org/10.1523/JNEUROSCI.3135-07.2007.
49. Rofo, F., Metzendorf, N.G., Saubi, C., Suominen, L., Godec, A., Sehlin, D., Syvänen, S., and Hultqvist, G. (2022). Blood-brain barrier penetrating neprilysin degrades monomeric amyloid-beta in a mouse model of Alzheimer's disease. Alzheimers Res. Ther. *14*, 180. https://doi.org/10.1186/s13195-022-01132-2.
50. Shi, Z., Zhang, K., Chen, T., Zhang, Y., Du, X., Zhao, Y., Shao, S., Zheng, L., Han, T., and Hong, W. (2020). Transcriptional factor ATF3 promotes liver fibrosis via activating hepatic stellate cells. Cell Death Dis. *11*, 1066. https://doi.org/10.1038/s41419-020-03271-6.
51. Baiocchini, A., Montaldo, C., Conigliaro, A., Grimaldi, A., Correani, V., Mura, F., Ciccosanti, F., Rotiroti, N., Brenna, A., Montalbano, M., et al. (2016). Extracellular Matrix Molecular Remodeling in Human Liver Fibrosis Evolution. PLoS One *11*, e0151736. https://doi.org/10.1371/journal.pone.0151736.
52. Jimenez-Loygorri, J.I., Villarejo-Zori, B., Viedma-Poyatos, A., Zapata-Munoz, J., Benitez-Fernandez, R., Frutos-Lison, M.D., Tomas-Barberan, F.A., Espin, J.C., Area-Gomez, E., Gomez-Duran, A., and Boya, P. (2024). Mitophagy curtails cytosolic mtDNA-dependent activation of cGAS/STING inflammation during aging. Nat. Commun. *15*, 830. https://doi.org/10.1038/s41467-024-45044-1.
53. Farmer, B.C., Williams, H.C., Devanney, N.A., Piron, M.A., Nation, G.K., Carter, D.J., Walsh, A.E., Khanal, R., Young, L.E.A., Kluemper, J.C., et al. (2021). APOEpsilon4 lowers energy expenditure in females and impairs glucose oxidation by increasing flux through aerobic glycolysis. Mol. Neurodegener. *16*, 62. https://doi.org/10.1186/s13024-021-00483-y.
54. Lee, H., Cho, S., Kim, M.J., Park, Y.J., Cho, E., Jo, Y.S., Kim, Y.S., Lee, J.Y., Thoudam, T., Woo, S.H., et al. (2023). ApoE4-dependent lysosomal cholesterol accumulation impairs mitochondrial homeostasis and oxidative phosphorylation in human astrocytes. Cell Rep. *42*, 113183. https://doi.org/10.1016/j.celrep.2023.113183.
55. Lee, S., Devanney, N.A., Golden, L.R., Smith, C.T., Schwartz, J.L., Walsh, A.E., Clarke, H.A., Goulding, D.S., Allenger, E.J., Morillo-Segovia, G., et al. (2023). APOE modulates microglial immunometabolism in response to age, amyloid pathology, and inflammatory challenge. Cell Rep. *42*, 112196. https://doi.org/10.1016/j.celrep.2023.112196.
56. Shimano, H., and Sato, R. (2017). SREBP-regulated lipid metabolism: convergent physiology - divergent pathophysiology. Nat. Rev. Endocrinol. *13*, 710–730. https://doi.org/10.1038/nrendo.2017.91.
57. de Leeuw, S.M., Kirschner, A.W.T., Lindner, K., Rust, R., Budny, V., Wolski, W.E., Gavin, A.C., Nitsch, R.M., and Tackenberg, C. (2022). APOE2,

E3, and E4 differentially modulate cellular homeostasis, cholesterol metabolism, and inflammatory response in isogenic iPSC-derived astrocytes. Stem Cell Rep. *17*, 1229–1231. https://doi.org/10.1016/j.stemcr.2022.03.018.

58. Blanchard, J.W., Akay, L.A., Davila-Velderrain, J., von Maydell, D., Mathys, H., Davidson, S.M., Effenberger, A., Chen, C.Y., Maner-Smith, K., Hajjar, I., et al. (2022). APOE4 impairs myelination via cholesterol dysregulation in oligodendrocytes. Nature *611*, 769–779. https://doi.org/10.1038/s41586-022-05439-w.

59. Sullivan, P.M., Mezdour, H., Aratani, Y., Knouff, C., Najib, J., Reddick, R.L., Quarfordt, S.H., and Maeda, N. (1997). Targeted replacement of the mouse apolipoprotein E gene with the common human APOE3 allele enhances diet-induced hypercholesterolemia and atherosclerosis. J. Biol. Chem. *272*, 17972–17980. https://doi.org/10.1074/jbc.272.29.17972.

60. Knouff, C., Hinsdale, M.E., Mezdour, H., Altenburg, M.K., Watanabe, M., Quarfordt, S.H., Sullivan, P.M., and Maeda, N. (1999). Apo E structure determines VLDL clearance and atherosclerosis risk in mice. J. Clin. Investig. *103*, 1579–1586. https://doi.org/10.1172/JCI6172.

61. Johnson, C.N., Lysaker, C.R., McCoin, C.S., Evans, M.R., Thyfault, J.P., Wilkins, H.M., Morris, J.K., and Geiger, P.C. (2024). Skeletal muscle proteome differs between young APOE3 and APOE4 targeted replacement mice in a sex-dependent manner. Front. Aging Neurosci. *16*, 1486762. https://doi.org/10.3389/fnagi.2024.1486762.

62. Pantazis, C.B., Yang, A., Lara, E., McDonough, J.A., Blauwendraat, C., Peng, L., Oguro, H., Kanaujiya, J., Zou, J., Sebesta, D., et al. (2022). A reference human induced pluripotent stem cell line for large-scale collaborative studies. Cell Stem Cell *29*, 1685–1702.e22. https://doi.org/10.1016/j.stem.2022.11.004.

63. Cameron, K., Tan, R., Schmidt-Heck, W., Campos, G., Lyall, M.J., Wang, Y., Lucendo-Villarin, B., Szkolnicka, D., Bates, N., Kimber, S.J., et al. (2015). Recombinant Laminins Drive the Differentiation and Self-Organization of hESC-Derived Hepatocytes. Stem Cell Rep. *5*, 1250–1262. https://doi.org/10.1016/j.stemcr.2015.10.016.

64. Peters, D.T., Henderson, C.A., Warren, C.R., Friesen, M., Xia, F., Becker, C.E., Musunuru, K., and Cowan, C.A. (2016). Asialoglycoprotein receptor 1 is a specific cell-surface marker for isolating hepatocytes derived from human pluripotent stem cells. Development *143*, 1475–1481. https://doi.org/10.1242/dev.132209.

65. Fuller, K.N.Z., McCoin, C.S., Stierwalt, H., Allen, J., Gandhi, S., Perry, C.G.R., Jambal, P., Shankar, K., and Thyfault, J.P. (2022). Oral combined contraceptives induce liver mitochondrial reactive oxygen species and whole-body metabolic adaptations in female mice. J. Physiol. *600*, 5215–5245. https://doi.org/10.1113/JP283733.

66. McCoin, C.S., Von Schulze, A., Allen, J., Fuller, K.N.Z., Xia, Q., Koestler, D.C., Houchen, C.J., Maurer, A., Dorn, G.W., Shankar, K., et al. (2019). Sex modulates hepatic mitochondrial adaptations to high-fat diet and physical activity. Am. J. Physiol. Endocrinol. Metab. *317*, E298–E311. https://doi.org/10.1152/ajpendo.00098.2019.

67. Graw, S., Tang, J., Zafar, M.K., Byrd, A.K., Bolden, C., Peterson, E.C., and Byrum, S.D. (2020). proteiNorm - A User-Friendly Tool for Normalization and Analysis of TMT and Label-Free Protein Quantification. ACS Omega *5*, 25625–25633. https://doi.org/10.1021/acsomega.0c02564.

STAR★METHODS

KEY RESOURCES TABLE

REAGENT or RESOURCE	SOURCE	IDENTIFIER
Antibodies		
Rabbit Monoclonal anti-ALB	Abcam	ab207327; RRID:AB_2755031
Rabbit Monoclonal anti-APOE	Abcam	ab183597; RRID:AB_3331650
Rabbit Monoclonal anti-ASGR1	Abcam	ab254261; RRID:AB_3718141
Rabbit Monoclonal anti-CYP27A1	Abcam	ab126785; RRID:AB_11128459
Rabbit Monoclonal anti-HNF4A	Abcam	ab92378; RRID:AB_10562973
Rabbit Monoclonal anti-NANOG	Abcam	ab109250; RRID:AB_10863442
Rabbit Monoclonal anti-OCT4	Abcam	ab181557; RRID:AB_2687916
Rabbit Monoclonal anti-SOX17	Abcam	ab224637; RRID:AB_2801385
Rabbit Monoclonal anti-FDFT1	Proteintech	83020-1-RR; RRID:AB_3670761
Rabbit Monoclonal anti-CS	Cell Signaling	Cat #14309; RRID:AB_2665545
Rabbit Monoclonal anti-HDAC1	Cell Signaling	Cat #34589; RRID:AB_2756821
Rabbit Monoclonal anti-HK1	Cell Signaling	Cat #2024; RRID:AB_2116996
Rabbit Monoclonal anti-PGAM1	Cell Signaling	Cat #12098; RRID:AB_2736922
Goat Anti-Rabbit IgG (H + L)-HRP Conjugate Secondary	Bio-Rad	Cat #172019
Goat Polyclonal anti-Rabbit Secondary, DyLight™ 488	Invitrogen	Cat #35552
Chemicals, peptides, and recombinant proteins		
mTeSR™ Plus	STEMCELL Technologies	Cat #100-0276
CellAdhere™ Laminin 521 (LN521)	STEMCELL Technologies	Cat #200-0117
ReLeSR™	STEMCELL Technologies	Cat #100-0483
Y-27632	STEMCELL Technologies	Cat #72304
CHIR99021	STEMCELL Technologies	Cat #72052
RPMI 1640	Gibco	Cat #11875093
B-27™ Supplement	Gibco	Cat #17504044
Penicillin-Streptomycin	Gibco	Cat #15070063
1X PBS pH 7.4	Gibco	Cat #10010023
DMEM/F-12	Gibco	Cat #11320033
TrypLE™ Express	Gibco	Cat # 12605010
1X HBSS	Gibco	Cat #14175095
HCM™ Hepatocyte Culture Medium BulletKit®	Lonza	Cat #CC-3198
Activin A	MedChemExpress	Cat #HY-P70311AF
bFGF	MedChemExpress	Cat #HY-P701242
BMP4	MedChemExpress	Cat #HY-P7007
HGF	MedChemExpress	Cat #HY-P700604
Oncostatin M	MedChemExpress	Cat #HY-P74662
Seahorse XF DMEM Assay Medium Pack, pH 7.4	Agilent	103680-100
DMSO	Millipore	D8418-100ML
RIPA Lysis Buffer	Millipore	20–188
HEPES	Millipore	391340-25GM
Dexamethasone	Sigma	265005-100MG

(*Continued on next page*)

Continued

REAGENT or RESOURCE	SOURCE	IDENTIFIER
Tween® 20	Sigma	P1379-100ML
Sucrose	Sigma	S0389-500G
Mannitol	Sigma	M9647-500G
Tris	Sigma	20-160
EDTA	Sigma	E9884-100G
EGTA	Sigma	E3889-25G
BSA	Sigma	810533
$MgCl_2$	Sigma	M8266-100G
Glucose	Sigma	G7021-100G
KH_2PO_4	Sigma	P0662-500G
Palmitoyl-coenzyme A	Sigma	P9716-10MG
Pyruvate	Sigma	P5280-100G
Malate	Sigma	M1000-100G
ADP	Sigma	A2754-500MG
FCCP	Sigma	C2920-10MG
Succinate	Sigma	398055-500G
Rotenone	Sigma	557368-1GM
Antimycin A	Sigma	A8674-25MG
TMPD	Sigma	T7394-5G
Ascorbate	Sigma	A4034-100G
Sodium Azide	Sigma	71289-5G
Amido Black	Sigma	A8181-1EA
Paraformaldehyde	Sigma	158127-100G
Triton™ X-100	Sigma	T8787-100ML
Pierce™ Protease Inhibitor Tablets	Thermo Scientific	Cat #A32965
SuperSignal West Femto	Thermo Scientific	Cat #34095
SuperSignal West Dura	Thermo Scientific	Cat # 34075
4-15% Criterion TGX Gels	Bio-Rad	5671083, 5671084, 5671085
PVDF Membranes	Bio-Rad	1620177
Animal-Free Blocker	Vector Laboratories	SP-5030-250
HCS LipidTOX™ Red Neutral Lipid Stain	Invitrogen	Cat #H34476
Hoechst 33342, trihydrochloride trihydrate	Invitrogen	Cat #H3570
Tetramethyl Rhodamine, Ethyl Ester, Perchlorate (TMRE)	Invitrogen	Cat #T669
MitoSOX™	Invitrogen	Cat #M36007
Amplex™ Red	Invitrogen	Cat #A12222
Rhod-2, AM	Invitrogen	Cat #R1244
Critical commercial assays		
Human Apolipoprotein E ELISA	Invitrogen	Cat #EHAPOE
Seahorse XF Cell Mito Stress Test Kit	Agilent	103015-100
Seahorse XF Glycolysis Stress Test Kit	Agilent	103020-100
Seahorse XF Glucose/Pyruvate Oxidation Stress Test Kit	Agilent	103673-100
Seahorse XF Long Chain Fatty Acid Oxidation Stress Test Kit	Agilent	103672-100
Pierce™ BCA Protein Assay Kit	Thermo Scientific	Cat # 23227

(*Continued on next page*)

Continued		
REAGENT or RESOURCE	SOURCE	IDENTIFIER
Deposited data		
"APOE4 drives widespread changes to the hepatic proteome and alters metabolic function" - iScience", Mendeley Data, V1, https://doi.org/10.17632/yzh2nz7xyy.1	MSV000100053 (Proteomics, MassIVE)	NA
Experimental models: Cell lines		
JIPSC001162 (*APOE3* REV/REV) (A)	Jackson Laboratory	JIPSC001162
JIPSC001150 (*APOE4* SNV/SNV) (A)	Jackson Laboratory	JIPSC001150
JIPSC001268 (*APOE3* REV/REV) (B)	Jackson Laboratory	JIPSC001268
JIPSC001142 (*APOE4* SNV/SNV) (B)	Jackson Laboratory	JIPSC001142
Experimental models: Organisms/strains		
APOE3 (B6.129P2-*Apoe*$^{tm2(APOE*3)Mae}$ N8)	Taconic Biosciences	1548-F, 1548-M; RRID:IMSR_TAC:1548
APOE4 (B6.129P2-*Apoe*$^{tm3(APOE*4)Mae}$ N8)	Taconic Biosciences	1549-F, 1549-M; RRID:IMSR_TAC:1549
Software and algorithms		
GraphPad Prism 10.6.1	GraphPad Software	https://www.graphpad.com/
Fiji (ImageJ)	Open Access	https://imagej.net/
BioRender	Science Suite Inc.	https://www.biorender.com/
Image Lab 6.1	Bio-Rad	https://www.bio-rad.com/
BioTek Gen5 Software	Agilent	https://www.agilent.com/
Spectronaut® 18.3	Biognosys	https://biognosys.com/software/spectronaut/
MitoCarta3.0	Broad Institute	https://www.broadinstitute.org/mitocarta/mitocarta30-inventory-mammalian-mitochondrial-proteins-and-pathways
KEGG: Kyoto Encyclopedia of Genes and Genomes	Kanehisa Laboratories	https://www.genome.jp/kegg/
Search Tool for the Retrieval of Interacting Genes/Proteins (STRING) 12.0	STRING Consortium	https://string-db.org/
Ingenuity Pathway Analysis (IPA)	QIAGEN	https://digitalinsights.qiagen.com/
Excel	Microsoft	https://www.microsoft.com/en-us/microsoft-365/excel
Other		
Standard Chow Diet	Teklad Global Rodent Diet®	Cat #8604
Orbitrap Exploris 480 LC-MS System	Thermo Scientific	N/A
Seahorse XFe96 Analyzer	Agilent	N/A
Seahorse XF Pro Analyzer	Agilent	N/A
BioTek Cytation 1	Agilent	N/A
ChemiDoc XRS Imaging System	Bio-Rad	N/A
Infinite 200 PRO	Tecan	N/A

EXPERIMENTAL MODEL AND STUDY PARTICIPANT DETAILS

Animals

Male and female homozygous *APOE3* (B6.129P2-*Apoe*$^{tm2(APOE*3)Mae}$ N8) and *APOE4* (B6.129P2-*Apoe*$^{tm3(APOE*4)Mae}$ N8) targeted replacement (TR) mice were purchased from Taconic Biosciences (Germantown, NY) for this study at ~2 months of age (n = 8 per group for genotype and sex). These *APOE* TR mice were previously generated by removing and replacing the endogenous mouse *Apoe* gene with the human *APOE* gene.[59,60] Mice were maintained on a standard chow diet (Teklad Global Rodent Diet, 8604) for the entire study and housed at ~25°C with a standard 12-h light/dark cycle. Mice were aged to 4 months before the administration of 90 mg/kg ketamine and 10 mg/kg xylazine followed by euthanasia. Liver tissue was collected immediately following euthanasia and used for mitochondrial isolation or stored at −80°C. Data from the mice used in this study were also used in another publication focused on skeletal muscle metabolism.[61] Animal work and protocols were conducted under approval from the Institutional Animal

Care and Use Committee at the University of Kansas Medical Center, Assurance Number: A3237-01. Experimenters were blinded until the end of the study for data analysis. A total of 16 *APOE3* and 16 *APOE4* mice were examined with equal sex distribution.

Human induced pluripotent stem cell culture

CRIPSR-Cas9 gene edited isogenic human induced pluripotent stem cells (iPSCs) homozygous for *APOE3* or *APOE4* were obtained from The Jackson Laboratory (JAX). These iPSCs were generated as previously described from the KOLF2.1J parental male cell line.[62] Two pairs of isogenic iPSCs were used in this study, with Pair A consisting of JIPSC001162 (*APOE3* REV/REV) and JIPSC001150 (*APOE4* SNV/SNV), and Pair B consisting of JIPSC001268 (*APOE3* REV/REV) and JIPSC001142 (*APOE4* SNV/SNV). Cells were cultured at 37°C and 5% CO_2 with mTeSR Plus (STEMCELL Technologies) and maintained on CellAdhere Laminin 521 (LN521) (STEMCELL Technologies) matrix coated culture plates (TPP). iPSCs were passaged using ReLeSR (STEMCELL Technologies), once they reached approximately 70–90% confluency. All iPSCs used in experiments were kept below passage 20.

METHOD DETAILS

Generation of hepatocyte-like cells

Differentiation of iPSCs to hepatocyte-like cells (iHLCs) was carried out using a combination of two previously described protocols with minor modifications.[63,64] Basal medium (BDM) for differentiation was generated by combining RPMI 1640 (Gibco) with B-27 supplement (Gibco) and penicillin-streptomycin (final concentration 5 U/mL and 5 μg/mL). This was then used for subsequent differentiation medias.

On day 1, nearly confluent iPSCs were passaged onto LN521 coated culture plates (TPP) at a density of $2.5x10^4$ cells/cm^2 in mTeSR Plus with 10 μM Y-27632 ROCK inhibitor (STEMCELL Technologies). The following day media was substituted with fresh definitive endoderm (DE) media which contained BDM supplemented with 100 ng/mL Activin A (MedChemExpress) and 3 μM CHIR99021 (STEMCELL Technologies). Fresh DE media was replaced daily until day 5, after which the cells were cultured in hepatic endoderm (HE) media consisting of BDM supplemented with 5 ng/mL basic fibroblast growth factor (bFGF) (MedChemExpress), 20 ng/mL bone morphogenetic protein 4 (BMP4) (MedChemExpress), and 0.5% DMSO. Full media changes were performed daily with HE media until day 10. Cells were then cultured for 5 days with full media changes in immature hepatocyte (IMH) media containing BDM plus 20 ng/mL hepatocyte growth factor (HGF) (MedChemExpress) and 0.5% DMSO. Finally, on day 15, the media was replaced with mature hepatocyte (MH) medium, followed by full media changes daily for another 10 days. MH media consisted of hepatocyte basal media (Lonza), SingleQuots supplements (Lonza), 20 ng/mL hepatocyte growth factor (HGF) (MedChemExpress), 20 ng/mL Oncostatin M (MedChemExpress), 100 nM dexamethasone (Sigma), and 0.5% DMSO. iHLCs used in experiments were between days 20–25 of differentiation.

For downstream functional assays, iHLCs were replated on day 20 of differentiation. Mature iHLCs were washed with 1X PBS (Gibco) and then dissociated with pre-warmed (37°C) TrypLE (Gibco) for 10–15 min. Cells in TrypLE were then diluted with DMEM/F-12 and passed through a 70 μm strainer. Cells were centrifuged for 5 min at 300 x g, resuspended in MH media containing 10 μM Y-27632 ROCK inhibitor (STEMCELL Technologies), and plated on LN521 coated plates. Plating density varied depending on downstream assays.

Mitochondrial isolation from whole liver

Mitochondria were isolated from fresh mouse liver samples as previously described.[65,66] Briefly, livers from mice were immediately placed in 8 mL of ice-cold mitochondrial isolation buffer (MIB) (220 mM mannitol, 70 mM Sucrose, 10 mM Tris, 1 mM EDTA, pH 7.4) and homogenized using a Teflon pestle on ice. Homogenates were then centrifuged at 1,500 x g for 10 min at 4°C to remove cell debris and fat. To remove additional debris, the supernatant was collected and passed through a gauze filter before being centrifuged at 8000 x g for 10 min at 4°C. The pellet was then resuspended on ice in 6 mL of MIB with a glass Dounce homogenizer before being centrifuged again at 6,000 x g for 10 min at 4°C. Resuspension of the new pellet was performed on ice in 4 mL of MIB plus 0.1% BSA using a glass Dounce homogenizer, followed by centrifugation at 4,000 x g for 10 min at 4°C. The final pellet containing mitochondria was resuspended in 500 μL of ice-cold MiR05 buffer (0.5 mM EGTA, 3 mM $MgCl_2$, 60 mM KMES, 20 mM glucose, 10 mM KH_2PO_4, 20 mM HEPES, 110 mM sucrose, 0.1% BSA, pH 7.1). A BCA assay (Thermo Scientific, 23227) was performed to determine protein content. Mitochondrial samples were then either immediately used for respiration analysis or frozen at −80°C.

Proteomics

Whole liver samples were lysed with RIPA buffer (Millipore) plus protease inhibitors (Thermo Scientific, A32965). Tissue lysates were then centrifuged at maximum speed for 10 min before the supernatant was transferred to a new tube. A BCA assay was performed to quantify protein concentration. Samples were then transferred to a new tube and diluted with fresh RIPA to 1 μg/μL (100 μg total). Protein content was determined from previously frozen isolated liver mitochondria samples which were diluted to 1 μg/μL (100 μg total). For proteomics analysis an $n = 4$ per group and sex were analyzed and samples were chosen randomly.

iHLCs were harvested for proteomics on day 21 of differentiation. Proteomic analysis was performed on two independent differentiation experiments using Pair A isogenics, referred to as Batch 1 and Batch 2. Plates containing iHLCs were placed on ice before media was removed and discarded. Cells were then washed once with ice-cold 1X PBS and then scraped in 1X PBS containing

protease inhibitors (Thermo Scientific, A32965). Cells were collected into 1.7 mL tubes and centrifuged at maximum speed for 5 min. The supernatant was removed, and the pellet was resuspended and lysed in 500 μL RIPA (Millipore) with protease inhibitors (Thermo Scientific, A32965). A BCA assay was used to determine protein content and samples were then diluted to 1 μg/μL (100 μg total) in fresh RIPA buffer.

Samples were then sent to the University of Arkansas Medical Center (UAMS) for proteomics. Briefly, protein samples were extracted using chloroform/methanol phase separation with a subsequent trypsin digestion to acquire peptides. Samples were then analyzed using liquid chromatography mass spectrometry (LC/MS) on a Orbitrap Exploris 480 (Thermo Scientific) with data independent acquisition (DIA).

APOE enzyme-linked immunosorbent assay (ELISA)

Quantification of APOE from mouse livers was completed using a commercially available ELISA kit (Invitrogen, EHAPOE). Mouse livers were dounce homogenized on ice in RIPA buffer (Millipore) with the addition of protease inhibitors (Thermo Scientific, A32965). Liver homogenates were then centrifuged at 12,500 x g for 10 min. Supernatants were collected in new tubes and diluted 1:100 in assay diluent buffer. The ELISA was completed per the manufacturer's instructions. Final concentrations were normalized to protein determined using a BCA assay (Thermo Scientific, 23227).

Western blotting

Lysates from cells and whole mouse livers were collected on ice and lysed using RIPA buffer (Millipore) plus protease inhibitors (Thermo Scientific, A32965). A BCA assay (Thermo Scientific, 23227) was performed, and an equal amount of protein was resolved on 4–15% Criterion TGX gels (Bio-Rad). Gels were transferred to PVDF membranes (Bio-Rad) and blocked overnight at 4°C with 5% bovine serum albumin (BSA) in 1X phosphate buffered saline with Tween (PBST). The albumin western blot was blocked with animal free blocking solution (Vector Laboratories, SP-5030-250). Primary antibodies diluted at 1:1000 were applied to the membranes and incubated overnight at 4°C. Blots were washed three times in 1X PBST and incubated at room temperature for 1 h with secondary antibodies diluted 1:2000 in 5% non-fat dry milk (NFDM) prepared in 1X PBST. Blots were then imaged using SuperSignal West Femto or West Dura ECL substrates (Thermo Scientific) on a ChemiDoc XRS imaging system (Bio-Rad). Amido black (Sigma) was used to stain total protein. Primary antibodies included ALB (Abcam, ab207327), APOE (Abcam, ab183597), ASGR1 (Abcam, ab254261), CS (Cell Signaling, #14309), CYP27A1 (Abcam, ab126785), FDFT1 (Proteintech, 83020-1-RR), HDAC1 (Cell Signaling, #34589), HK1 (Cell Signaling, #2024), HNF4A (Abcam, ab92378), NANOG (Abcam, ab109250), OCT4 (Abcam, ab181557), PGAM1 (Cell Signaling, #12098), and SOX17 (Abcam, ab224637).

Immunocytochemistry (ICC)

iHLCs on day 23 of differentiation were fixed using 4% paraformaldehyde (PFA) (Sigma) for 15 min. Cells were washed three times with 1X PBS (Gibco) before being permeabilized with 0.1% Triton X-100 (Sigma) for 10 min in 1X PBST. Cells were washed three times with 1X PBS (Gibco) and blocked for 1 h at room temperature with 1% BSA in 1X PBST. The blocking solution was removed, and cells were incubated overnight with primary antibodies at 4°C. The following day cells were washed with 1X PBS (Gibco) three times followed by a 1 h incubation at room temperature with secondary fluorophore conjugated antibodies. The nuclear counterstain Hoechst was used at a concentration of 2 μg/mL for 30 min. Finally, cells were washed three times with 1X PBS (Gibco) before being imaged on a BioTek Cytation 1 (Agilent). Primary antibodies included APOE diluted 1:400 (Abcam, ab183597), ASGR1 diluted 1:200 (Abcam, ab254261), and HNF4A diluted 1:200 (Abcam, ab92378). We used DyLight 488 conjugated secondary antibody (Invitrogen, 35552) at a concentration of 2 μg/mL.

Isolated mitochondria respiration

Liver mitochondrial oxygen consumption rates (OCR) were measured using a Seahorse XFe96 Analyzer (Agilent). Isolated mitochondria were diluted to 15–20 μg per 180 μL using mitochondrial assay solution (MAS) (220 mM Mannitol, 70 mM Sucrose, 10 mM K_2HPO_4, 5 mM $MgCl_2$, 2 mM HEPES, 1 mM EGTA, 0.2% fatty acid-free BSA). Mitochondria were loaded into Seahorse cell culture plates at 180 μL per well. The Seahorse plate was centrifuged at 1000 x g for 5 min with the brake set at 5. State 2 respiration rates were determined using palmitoyl-coenzyme A (PCoA, 10 μM) or 5 mM pyruvate and 5 mM malate. State 3 respiration was acquired after the addition of 4 mM ADP. Succinate was then injected at a concentration of 10 mM to acquire state 3S. The final addition of carbonyl cyanide-*p*-trifluoromethoxy phenylhydrazone (FCCP, uncoupled, 4 μM) assessed maximal respiratory flux. Respiration values were normalized to total protein amount loaded and across days of mitochondrial respiration analysis.

Cellular respiration

A Seahorse XF Pro Analyzer (Agilent) was used to determine iHLC OCR and extracellular acidification rates (ECAR). Cells were plated at a density of 35,000 per well on LN521 coated Seahorse cell culture plates. Substrates were successively injected to measure OCR or ECAR for different respiration rates. *Mitochondrial Stress Test*: Seahorse base medium contained 10 mM glucose, 2 mM glutamine, with injections A) 2 μM oligomycin B) and C) 0.5 μM FCCP D) 1 μM antimycin A and rotenone. *Glycolysis Stress Test:* Seahorse base medium contained 2 mM glutamine with injections A) 10 mM glucose B) 2 μM oligomycin C) 100 mM 2-deoxy-glucose (2-DG). *Electron Transport Chain Flux:* Medium was 1X MAS supplemented with 10 mM pyruvate/5 mM malate/4 mM ADP and 1 nM plasma

membrane permeabilization (PMP) reagent with injections A) 10 mM Succinate/1 μM rotenone B) 1 μM antimycin A C) 0.5 mM TMPD/1 mM ascorbate D) 50 mM azide. *Glucose/Pyruvate and LCFA Substrate Oxidation Stress Tests*: To determine substrate oxidation we used Seahorse base medium containing 10 mM glucose, 2 mM glutamine, and 1 mM pyruvate with the following injection scheme: A) assay medium or 2 μM UK5099 or 4 μM Etomoxir B) 2 μM oligomycin C) 0.5 μM FCCP D) 1 μM antimycin A and rotenone.

OCR and ECAR were measured following a 3-min mix after the addition of injections and were measured over 3 min three times. All data were analyzed using the Agilent Seahorse Wave software and Microsoft Excel.

LipidTOX imaging and quantification

To quantify lipid droplets (LDs) in iHLCs, we used HCS LipidTOX Red neutral lipid stain (Invitrogen, H34476). LD staining of iHLCs was done as specified in the manufacturer's instructions. Cells were re-plated at a density of 3.0 × 10 ^4 cells/well in a transparent-bottom 96-well plate (Agilent, 204626-100) and allowed to recover for one day. Cells were fixed with 4% PFA for 20 min at room temperature and then washed three times with 1X PBS (Gibco). 1X LipidTOX stain was subsequently added with Hoechst (Invitrogen) at a concentration of 2 μg/mL, and cells were incubated for 30 min at room temperature before imaging on a BioTek Cytation 1 (Agilent). Data was acquired and analyzed using BioTek Gen5 software (Agilent). We quantified the average number of LDs per cell in each field of view at 20× magnification using a software spot counting feature. We also quantified the average size (diameter) of LDs. Parameters for analysis included a cell size diameter cutoff of 30 μm and LD size cutoff of 0.2–5 μm.

Mitochondrial indicator assays

iHLCs were plated at a density of 2.0–3.0x10^4 cells/well of a transparent bottom 96 well plate (3603, Corning) and allowed to recover for one day. To assess mitochondrial membrane potential we used 200 nM tetramethyl rhodamine, ethyl ester (TMRE) (Invitrogen). Mitochondrial superoxide was measured with 500 nM MitoSOX™ Red (Invitrogen) and hydrogen peroxide (H_2O_2) was determined using 50 μM Amplex™ Red (Invitrogen) with 0.1 U/mL horseradish peroxidase (HRP). Levels of mitochondrial calcium (Ca^{2+}) were measured using 1 μM Rhod-2, AM (Invitrogen). Hoechst (Invitrogen) was used for normalization at a concentration of 10 μg/mL. Cells were stained with respective dyes diluted for 30 min at 37°C and then washed twice with 1X Hanks' Balanced Salt Solution (HBSS) (Gibco). Fluorescence intensity for each dye was read with a Tecan Infinite 200 PRO® and normalized to Hoechst. Representative images for TMRE were acquired at 20× magnification using a BioTek Cytation 1 (Agilent).

QUANTIFICATION AND STATISTICAL ANALYSIS

Proteomic data analysis

Data analysis of samples was completed using Spectronaut® software (Biognosys version 18.3). UniProt databases were used to identify both mouse (*Mus musculus*) and human (*Homo sapiens*) proteins. Quality control (QC) and normalization was carried out with proteiNorm.[67] MitoCarta3.0 was used to further identify mitochondrial-specific proteins in the isolated liver mitochondria samples.[20] Proteins with a p-value <0.05 were considered significant. QIAGEN Ingenuity Pathway Analysis (IPA) was used for pathway, upstream regulator, and comparison analysis. Proteins included in pathway analysis had a p-value cutoff of <0.2 for whole liver and isolated mitochondria samples, and <0.05 for iHLCs. For pathway analysis, a nominal p-value cutoff of <0.2 was applied to the mouse proteomic data to increase sensitivity in detecting coordinated biological trends. Pathways with a Z score of ≤ -2 and $\geq +2$ and a log fold change (logFC) of $\geq$1.3 were considered significant. Cross-referencing protein lists identified proteins involved in specific pathways or cellular functions with multiple databases including Kyoto Encyclopedia of Genes and Genomes (KEGG), Search Tool for the Retrieval of Interacting Genes/Proteins (STRING), and IPA. STRING analysis was also used to show selected protein interactions.

Statistical analysis

Values are shown in figures as mean ± SD. Data analysis was completed using GraphPad Prism 10 software and Microsoft Excel. Outliers were identified and removed from datasets using Grubbs' test with a significant alpha of 0.05. Significance for simple comparisons was calculated using an unpaired t test. For comparisons of multiple groups, we used a two-way analysis of variance (ANOVA) (factors were sex and genotype) followed by Fisher's Least Significant Difference (LSD) post-hoc test if significant interactions were identified. A cutoff p-value <0.05 was considered significant for all analyses. Pearson correlation analysis was used to assess correlations. All graphs and figures were generated using GraphPad Prism 10.6.1 software and BioRender.com.